in draining lymph nodes (LNs) in a CCR7-dependent manner (20). Corroborating this, a deficiency of CCR7 or its ligands, CCL19 and CCL21, leads to impaired DC migration into draining LNs and abnormal lymph node architecture in peripheral tissues (21, 22). In addition, a recent study indicates that steady-state trafficking of skin DCs to the draining LNs in peripheral tissues is also regulated by CCR7-mediated signaling (23). However, it is not known whether this commonly held paradigm of DC trafficking being driven by CCR7-mediated signaling holds true for DCs in the intestinal compartment as well.

In the present study we found that there are at least two LP-DC subsets in the intestinal LP of unperturbed mice and that they both require CCR7 for their constitutive migration to the MLNs. They vigorously ingest apoptotic IECs and, hence, are likely to correspond to the cells identified by Huang et al. (15) in rat mesenteric lymph. As suggested previously (15), LP-DCs can present IEC-associated Ags to $CD4^+$ T cells, inducing their differentiation into IL-4- and IL-10-producing cells. These results strongly indicate that LP-DCs bearing a unique immunomodulatory activity migrate constitutively to MLNs in a CCR7-dependent manner, thus generating a noninflammatory environment in the MLNs.

Materials and Methods

Mice

BALB/c mice were obtained from CLEA Japan. C57BL/6 mice were obtained from Japan SLC. Mice transgenic for a TCR that recognizes the $OVA_{323-339}$ peptide in the context of $I\text{-}A^d$ (DO 11.10 TCR-$\alpha\beta$ transgenic mice) on the BALB/c background were a gift from Dr. S. Ono (Osaka University Graduate School of Medicine, Osaka, Japan). The *plt/plt* mice on the B6 background were provided by Dr. H. Nakano (Duke University Medical Center, Raleigh, NC). CCR7-deficient mice on the C57BL/6 background were produced as previously described (21). All animal experiments were performed under an experimental protocol approved by the ethics review committee for animal experimentation of Osaka University Graduate School of Medicine.

Preparation of DCs from small intestinal LP, PPs, MLNs, and spleen

Small intestinal segments and PPs were treated with PBS containing 10% FCS, 20 mM HEPES, 100 U/ml penicillin, 100 μg/ml streptomycin, 1 mM sodium pyruvate, 10 mM EDTA, and 10 μg/ml polymyxin B (Calbiochem) for 30 min at 37°C to remove epithelial cells and were washed extensively with PBS. Small intestinal segments, PPs, MLNs, and spleen were digested with 400 Mandl units/ml collagenase D (Roche) and 10 μg/ml DNase I (Roche) in RPMI 1640/10% FCS with continuous stirring at 37°C for 45–90 min. EDTA was added (10 mM final concentration), and the cell suspension was incubated for an additional 5 min at 37°C. Cells were spun through a 15.5% Accudenz (Accurate Chemical & Scientific) solution to enrich for DCs. The obtained cells were incubated with FITC-conjugated anti-CD11b and PE-conjugated anti-CD11c after FcR blocking. DC subsets were sorted on the basis of their expression of CD11c and CD11b by FACSVantage SE (BD Biosciences). The purity of the sorted DCs was routinely >95%. For the morphological study, cytospin preparations from purified DC subsets were stained with May-Grunwald-Giemsa solution.

Double immunofluorescence staining of small intestinal LP

To determine the location of LP-DCs in the small intestinal LP, biotinylated anti-CD11c and FITC-conjugated anti-CD11b mAbs were applied overnight at 4°C to sections cut from frozen tissue. Samples were washed and then incubated with streptavidin-Alexa 594 (Molecular Probes) for 2 h at room temperature. To detect $CCR7^+$ DCs in the small intestinal LP, frozen sections of the small intestine were stained with rabbit anti-mouse CCR7 pAb, provided by Dr. K. Matsushima (University of Tokyo School of Medicine, Tokyo, Japan) and biotinylated anti-CD11c mAb overnight at 4°C. The sections were washed and then further incubated with Alexa 488-conjugated chicken anti-rabbit IgG Ab (Molecular Probes) and streptavidin-Alexa 594 for 2 h at room temperature. Immunohistochemical staining was analyzed with a Radiance 2100/Bio-Rad confocal laser microscope (Bio-Rad).

Flow cytometry

Fluorochrome-conjugated anti-CD11c (HL3), anti-CD11b (M1/70), and anti-CD8α (53-6.7) mAbs were used for DC staining. Anti-mouse CD16/CD32 (2.4G2) was used for FcR blocking. The expression of integrins was determined using mAbs to integrin α_L (CD11a; M17/4) and β_7 (M293). The expression of costimulatory molecules was determined using mAbs to B7-1 (CD80; 16-10A1), B7-2 (CD86; GL1), CD40 (3/23), and $I\text{-}A^d$ (AMS-32.1). These reagents were all purchased from BD Pharmingen. After the FcRs were blocked for 15 min at 4°C, the cells were stained for integrins, CD8α, CD11c, CD11b, and costimulatory molecules and then analyzed with a FACSCalibur (BD Biosciences). The DCs were identified by gating on the $CD11c^{high}$ cells. CCR7 expression by DCs was determined using the CCL19-Fc chimeric protein provided by Drs. K. Hieshima and O. Yoshie (Kinki University School of Medicine, Kinki, Japan).

RT-PCR for chemokine receptor expression

Total RNA was prepared from freshly isolated LP-DC using TRIzol (Invitrogen Life Technologies). RT of total RNA was conducted using oligo$(dT)_{18}$ primer and SensiScript reverse transcriptase (Qiagen). PCR was conducted using primer pairs for CCR1 (sense, AGAAGCCTACCCCA CAAC; antisense, TGGCCAGGTATCTGTCAA), CCR7 (sense, GGTGT GCCTCTGCCAAGA; antisense, TGCCAAAGATGCCCTTAC), CCR9 (sense, TGCTACTGGAGACAACTTCG; antisense, CTCCTCAGAACT GCAGTTAC), and β-actin (sense, ATGGATGACGATATCGCT; antisense, ATGAGGTAGTCTGTCAGGT) and Ex-*Taq* polymerase (Takara Shuzo). The PCR conditions were 30 cycles at 97, 57, and 72°C for 30 s each, and the products were analyzed on agarose gels.

Chemotaxis assays

All cell suspensions and chemokine dilutions were made in RPMI 1640 containing 0.5% low endotoxin BSA (Sigma-Aldrich). The chemokine CCL21 was purchased from Techne. Chemotactic assays were performed as previously described (24). Two hours after the start of migration, the inserts were removed. Migrated DCs were identified on a FACSCalibur using FITC-conjugated anti-CD11b mAb and PE-conjugated anti-CD11c mAb.

Real-time chemotaxis assay

Real-time chemotaxis assays were performed as previously described (25). To count the migrated cells in each channel, images of the cells in each channel were digitally recorded onto a computer hard disk with time-lapse intervals of 60 s.

Detection of apoptotic IECs in MLN-DCs

To detect IECs-derived apoptotic DNA in DCs, cytospin preparations from FACS-sorted MLN-DCs were fixed with 1% paraformaldehyde and stained using an ApopTag peroxidase in situ apoptosis detection kit (Serologicals) Detection of alkaline phosphatase activity in the FACS-sorted $CD11c^{high}CD8\alpha^{int}\alpha_L{}^{low}\beta_7{}^{high}$ MLN-DC subset was performed using the Vector Red Alkaline Phosphatase Substrate Kit I (Vector Laboratories).

Electron microscopy

Isolated cells were spun at 400 × *g* and fixed in 1% in glutaraldehyde in 0.1 M phosphate buffer for 1 h at 4°C. After being washed, the cells were embedded in 2% agarose gel and postfixed in 2% osmium tetroxide in 0.1 M phosphate buffer for 2 h at 4°C. The fixed samples were then dehydrated in a graded ethanol series, infiltrated with propylene oxide, and embedded in Quetol 812 epoxy resin. Ultrathin sections were stained with 2% uranyl acetate and Reynold's lead citrate, then examined using a JEOL JEM-1230 electron microscope.

In vitro uptake of CFSE-labeled apoptotic epithelial cells by DCs

Small IECs were obtained as described previously (26). IECs were then labeled with CFSE (Molecular Probes) at a concentration of 5 μM for 5 min at 37°C and cultured for 4 h to induce spontaneous apoptosis. Enriched DCs were mixed with CFSE-labeled apoptotic IECs and cultured for 4 h at 37°C. After the coculture, cells were stained with PE-conjugated anti-CD11c mAb and allophycocyanin-conjugated anti-CD11b mAb to identify the DC subsets. The uptake of apoptotic IECs by DCs was evaluated by FACSCalibur.

Analysis of $CD4^+$ T cell proliferation and cytokine production

IECs obtained as described above were loaded with OVA (Sigma-Aldrich) by osmotic shock (27). They were then cocultured with DCs for 4 h, and

the DC subsets were subsequently sorted on the basis of their expression of CD11c and CD11b. Purified DCs (5×10^3) and DO11.10 OVA TCR-transgenic T cells (1×10^5) were mixed in 96-well plates (1/20). After 7 days, the cells were collected and stained with anti-mouse DO11.10 TCR (KJ1-26; Caltag Laboratories) and anti-mouse CD4 (RM4-5) mAbs. Dead cells were excluded using 7-aminoactinomycin D (Sigma-Aldrich). T cell proliferation was measured by CFSE dilution. To examine cytokine secretion, DO11.10 $CD4^+$ T cells were cocultured with IEC-OVA-containing DCs for 14 days (two-round stimulation with IEC-OVA-containing DCs with a 7-day interval). The T cells were then washed and restimulated for 6 h with anti-CD3 mAb in the presence of monensin (BD Pharmingen). Intracellular cytokine staining was performed according to the manufacturer's instructions (BD Pharmingen).

Results

Small intestinal LP contains two distinct DC subsets

We first determined the localization of LP-DC subsets in the small intestine by immunohistochemistry. As shown in Fig. 1*A*, cells that were $CD11b^-/CD11c^+$ (open arrowheads) and $CD11b^+/CD11c^+$ (filled arrowheads) were readily recognizable in the LP, indicating that the small intestinal LP contains at least two phenotypically distinguishable DC subsets.

We next attempted to isolate LP-DCs and successfully obtained substantial numbers of low density leukocytes from the LP ($1.95 \pm 0.5 \times 10^6$ cells/mouse; $n = 34$), of which the $CD11c^+$ DCs constituted ~10–15%. Among these cells, at least two LP-DC subsets could be recognized on the basis of their different CD11c/CD11b expression patterns: $CD11c^{high}CD11b^{low}$ (R1; 4.9 ± 2.0% of low density cells) and $CD11c^{high}CD11b^{high}$ (R2; 8.4 ± 2.0%; Fig. 1*B*). The remaining cells, which were $CD11c^{int}CD11b^{high}$, consisted mainly of cells that contained eosinophilic granules (J.-H. Seoh and M. H. Jang, manuscript in preparation). The $CD11c^{high}$ LP-DC subsets were heterogeneous in their CD8α expression, in that the $CD11c^{high}CD11b^{low}$ subset expressed CD8α at an intermediate level ($CD8\alpha^{int}$), whereas the $CD11c^{high}CD11b^{high}$ subset was $CD8\alpha^-$ (Fig. 1*B*). Thus, the phenotypes of the R1 and R2 subsets were $CD11c^{high}CD8\alpha^{int}CD11b^{low}$ and $CD11c^{high}CD8\alpha^-CD11b^{high}$, respectively.

These two subsets were found not only in the intestines of $Id2^{-/-}$ mice, which are completely deficient in PPs and ILFs (28), but also in the BALB/c small intestine from which PPs and ILFs had been surgically removed before the isolation procedure (data not shown), suggesting that they are indeed derived from the small intestinal LP and not PPs or ILFs. Interestingly, the freshly isolated R1 and R2 subsets both had few dendrites. The nuclear chromatin was not very condensed, and the cytoplasm was light blue to grayish when stained with May-Grunwald-Giemsa solution, suggesting that the LP-DCs were not fully mature (Fig. 1*C*).

The expression of costimulatory molecules also supported the idea that these cells were somewhat immature. As shown in Fig. 1*D*, LP-DCs showed substantially lower expression of MHC class II and CD40 than DCs from PPs and MLNs, indicating that they were less mature than other DCs in the intestinal compartment. Interestingly, however, the LP-DCs displayed a relatively high expression level of B7-2, as seen in PP-DCs, if not as high as that expressed by MLN-DCs, indicating that the LP-DCs may not be entirely immature but, rather, may constitute semimature subsets. The $CD11c^{high}$ LP-DC subsets were $DEC\text{-}205^+$, but $B220^-$ and $Gr\text{-}1^-$ (data not shown), indicating that they are distinct from plasmacytoid DCs (29) or the recently identified $CD70^+$ APCs (30) in the LP, both of which express readily detectable levels of DEC-205, B220, and Gr-1.

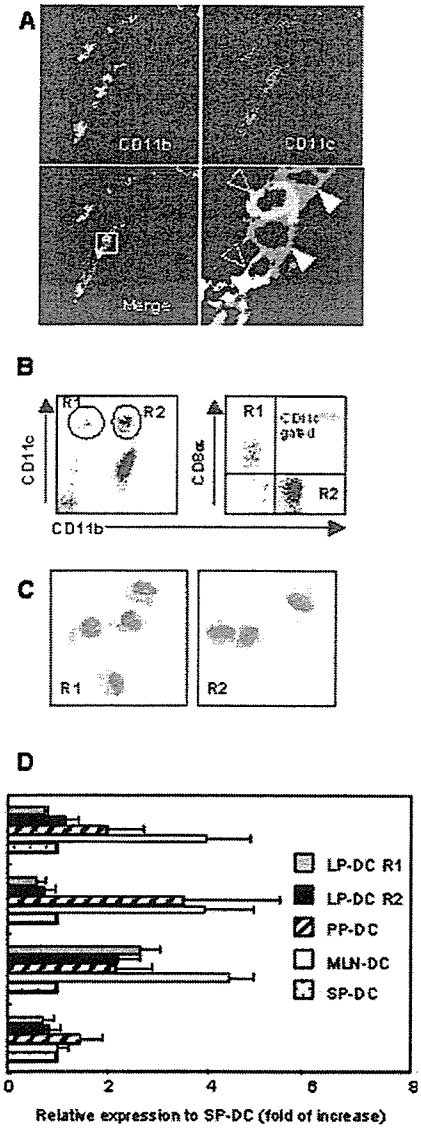

FIGURE 1. Identification of two DC subpopulations in the LP of the small intestine. *A*, Frozen sections of small intestine were fixed, stained with Abs specific for CD11b (green) and CD11c (red), and analyzed by confocal microscopy. Two cell subsets, $CD11b^-CD11c^+$ (red; open arrowheads) and $CD11b^+CD11c^+$ (yellow; filled arrowheads) were readily identifiable within the LP. *B*, Low density lamina propria cells were isolated from the small intestines of BALB/c mice and spun through a 15.5% Accudenz gradient. Enriched DCs were stained for CD8α, CD11b, and CD11c and analyzed by flow cytometry. *C*, Two DC subsets (R1 ($CD11c^{high}CD8\alpha^{int}CD11b^{low}$) and R2 ($CD11c^{high}CD8\alpha^-CD11b^{high}$)) were FACS-sorted based on their CD11c and CD11b expressions and stained with May-Grunwald-Giemsa. The R1 and R2 subsets had a morphology associated with highly motile cells. *D*, The LP-DC subsets had a semimature phenotype. DC subsets from LP, PPs, MLNs, and spleen (SP) were stained for CD11c, CD11b, and B7-1, B7-2, CD40, or $I\text{-}A^d$ and analyzed by flow cytometry. The expression levels are shown as the ratio of the mean fluorescence intensity (MFI) to the fluorescence intensity of SP-DCs.

LP-DC subsets express CCR7 and show directional migration toward CCL21

Although steady-state trafficking of DCs from the skin to the draining LNs is regulated by CCR7-mediated signaling (23), it remains to be established whether LP-DC trafficking is also regulated by a

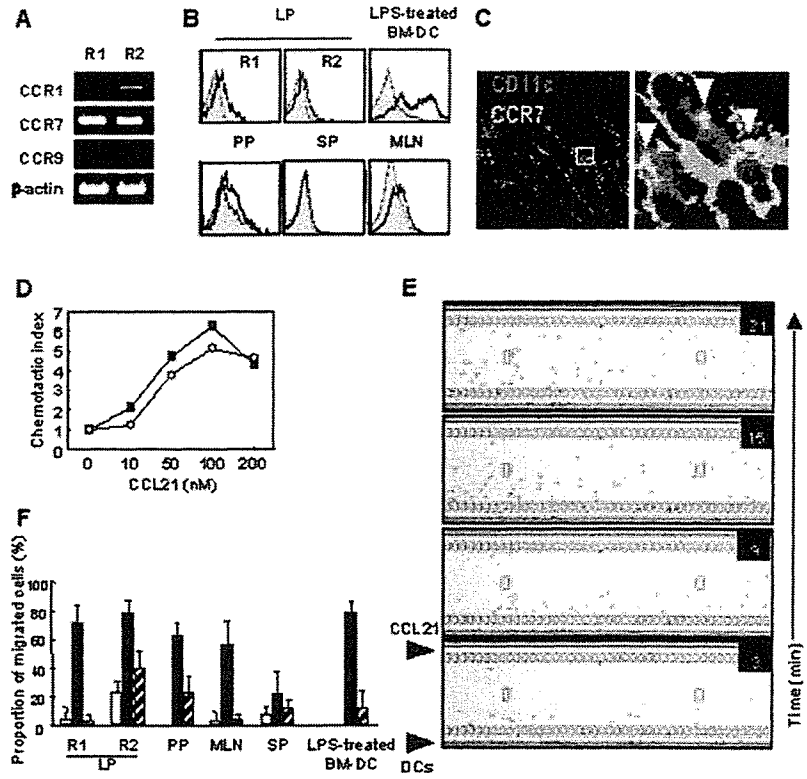

FIGURE 2. LP-DC subsets express CCR7 and show directional migration toward CCL21. *A*, Expression of CCR7 mRNA. cDNA was prepared from total RNA obtained from freshly FACS-sorted LP-DCs, and the expression of chemokine receptors was analyzed by semiquantitative PCR. *B*, Expression of CCR7 protein on the cell surface. DCs were stained for CCR7 using the CCL19-Fc chimera protein (□). LPS-stimulated bone marrow-derived DC was used as a positive control, and human Ig Fc protein served as a negative control (▨). *C*, Localization of $CCR7^+/CD11c^+$ DCs in the small intestinal LP. Frozen sections of the small intestine were fixed and stained with anti-CCR7 pAb and biotinylated anti-CD11c mAb. The sections were further incubated with Alexa 488-conjugated secondary Ab and streptavidin-Alexa 594. Arrows indicate $CCR7^+/CD11c^+$ cells. *D*, Chemotaxis analysis by Transwell. LP-DCs were placed in the upper well of a Transwell apparatus (5-μm pore size), and an increasing concentration of CCL21 was added to the lower well for 2 h. The migrated cells were stained for CD11c and CD11b, then analyzed by FACSCalibur. The proportion of migrated cells in each population was calculated as a fraction of the input population. The chemotactic index is shown as the ratio of the proportion of cells that migrated in the presence of chemokine to the proportion that migrated in the absence of chemokine. ■, R1 subset; ○, R2 subset. *E*, Time-lapse video monitoring of chemotaxis. Isolated LP-DCs were applied to the microchemotaxis chamber. After aligning the cells on the edge of the microchannel of the chamber, CCL21 (10 μM) was applied to the opposite side of the microchannel (see *top* of each frame), so that a concentration gradient of the chemokine formed from the top to the bottom of the channel. The migration of cells in the microchannel was subsequently monitored at 6-min intervals. Note that a significant fraction of the cells had begun migrating from the bottom to the top of the field 15–21 min after the addition of CCL21. *F*, Quantitative evaluation of chemotactic responses to CCL21. Data are shown as the proportion of cells that migrated across the microchannel to the total cells in the assay area. □, Medium alone; ■, CCL21; ▨, CCL21 with PTX treatment. The data are representative of at least three independent experiments.

CCR7-dependent mechanism. We thus examined CCR7 expression in LP-DCs. In the R1 ($CD11c^{high}CD11b^{low}$) and R2 ($CD11c^{high}CD11b^{high}$) subsets, CCR7 mRNA was highly expressed, whereas CCR9 mRNA was absent (Fig. 2*A*). Consistent with this, LP-DCs were $CCR7^+$, as evidenced by their binding of a CCL19-fusion protein (Fig. 2*B*), and $CD11c^+$ DCs expressing CCR7 were readily detectable in the LP by immunohistochemistry (Fig. 2*C*). Furthermore, in vitro, the $CD11c^{high}$ LP-DCs efficiently migrated through Transwell inserts in response to CCL21 with the typical bell-shaped dose-response curve that is characteristic of chemotaxis (Fig. 2*D*). To verify that this reflects directional, but not random, migration, we adopted an optical chemotaxis assay system that allows time-lapse video monitoring of cell behavior in silicon-coated microchannels (25). As shown in Fig. 2*E* and supplemental movie A,[5] LP-DCs moved swiftly along the CCL21 concentration gradient, verifying that they can migrate directionally toward a CCL21 source as a result of expressing functional CCR7. Compared with DCs from other tissues, LP-DCs showed much stronger chemotaxis toward CCL21 than splenic DCs (SP-DCs), but their chemotaxis was comparable to that seen in MLN-DCs and PP-DCs (Fig. 2*F*). LPS-stimulated, bone marrow-derived DCs responded to CCL21 much like the LP-DC subsets. In all these cell types, CCL21-mediated migration was significantly blocked by pertussis toxin. These data indicate that LP-DCs with relatively immature morphology and phenotype can migrate toward CCL21 as efficiently as mature DCs without deliberate inflammatory stimulation.

LP-DCs migrate to MLNs in a CCR7-dependent manner

We next investigated whether LP-DCs could be identified in the MLNs and, if so, whether their migration was dependent on CCR7. Because a recent study indicated that DC migrants to lymph nodes could be discriminated by their surface phenotype (31), we first compared the expressions of various surface markers on the $CD11c^{high}$ DCs obtained from the LP, PPs, MLNs, and spleen. As shown in Fig. 3*A*, LP-DCs highly expressed β_7 integrin compared with other DCs. In this regard, LP-DCs contained $CD8\alpha^{int}\beta_7^{high}$ and $CD8\alpha^-\beta_7^{high}$ subpopulations, which correspond to the R1 and

[5] The online version of this article contains supplemental material.

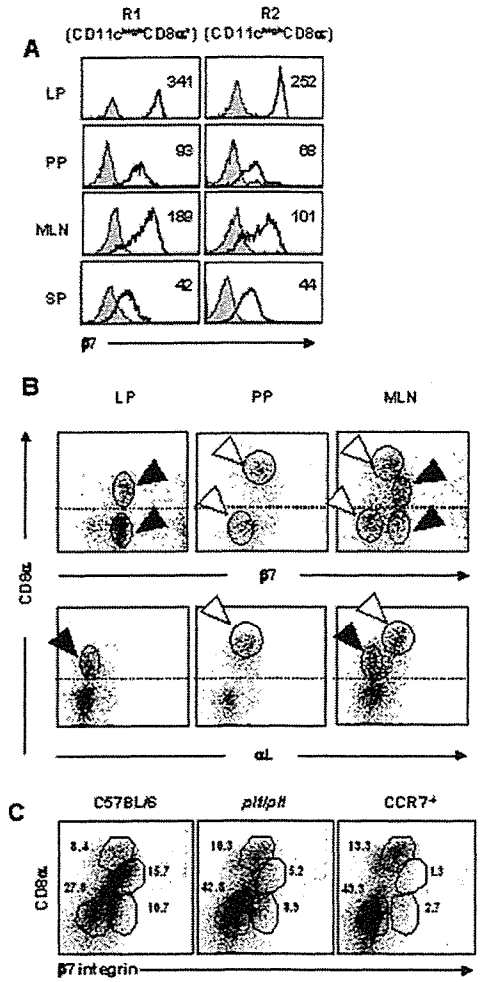

FIGURE 3. Apparent CCR7 dependency of the CD8$\alpha^{int}\beta_7^{high}$ and CD8$\alpha^-\beta_7^{high}$ subsets in MLNs. *A*, LP-DCs highly expressed β_7 integrin compared with other DCs. Low density cells from the LP were stained for CD11c, CD8α, and β_7 integrin, and the histogram profiles were acquired after gating on CD11c^{high}CD8α^+ DCs (R1) or CD11c^{high}CD8α^- DCs (R2). ▨, Isotype controls; □, stained cells. The numbers in the histograms indicate the MFI. *B*, LP-DCs and PP-DCs appear to constitute the MLN-DCs. Low density cells from the LP were double stained for CD8α/integrin β_7 or for CD8α/integrin α_L. FACS profiles were acquired after gating on the CD11c^{high} cells. Based on the CD8α/integrin β_7 double staining, the MLN-DCs consisted of four recognizable subsets, with two of them phenotypically corresponding to LP-DCs (filled arrowheads) and the remaining two corresponding to PP-DCs (open arrowheads). A similar observation was made with CD8α/integrin α_L double staining; MLN-DCs showed two CD8α^+ subsets, one of which corresponded phenotypically to an LP-DC subset (filled arrowhead) and the other to a PP-DC subset (open arrowhead). *C*, CD8$\alpha^{int}\beta_7^{high}$ and CD8$\alpha^-\beta_7^{high}$ LP-DCs were significantly fewer in the MLNs of *plt/plt* mice and were almost absent from the MLNs of CCR7-deficient mice. Numbers indicate the percentage of each subset within gated CD11c^{high} cells.

R2 subsets, respectively, and the PP-DCs had CD8$\alpha^{high}\beta_7^{int}$ and CD8$\alpha^-\beta_7^{low}$ populations. In contrast, the MLN-DCs contained all four surface phenotypes, supporting the possibility that LP-DCs and PP-DCs enter the MLNs to make up the four different DC subsets there (Fig. 3*B*). Furthermore, the examination of α_L expression in CD8α^+ DCs revealed that those in the LP expressed relatively low levels of α_L (CD8$\alpha^{int}\alpha_L^{low}$), whereas those in PPs expressed high levels of α_L (CD8$\alpha^{high}\alpha_L^{high}$), and the MLN-DCs consisted of both populations (Fig. 3*B*). These observations thus suggest that the MLNs collect phenotypically different DCs from the LP and PPs, in accordance with the MLNs being the draining LNs of the LP and PPs.

We next asked whether these intestinal DCs enter the draining MLNs in a manner dependent on CCR7. For this purpose, we examined MLN-DCs in wild-type C57BL/6 mice; in C57BL/6-*plt/plt* mice, which are deficient in CCL19/CCL21-Ser (22); and in CCR7-deficient mice (21) that had been backcrossed to the C57BL/6 genetic background. As shown in Fig. 3*C*, the CD8$\alpha^{int}\beta_7^{high}$ and CD8$\alpha^-\beta_7^{high}$ subsets (R1 and R2 in the LP, respectively) represented subsets of the MLN-DCs of wild-type mice (15.7 and 10.7% of the total CD11c^{high} DCs, respectively), but these subsets were significantly less prominent (5.2 and 8.9%) in the MLNs of *plt/plt* mice, which lack CCL21-Ser, but express CCL21-Leu, in their lymphatics, and were almost totally absent (1.3 and 2.7%) in the MLNs of CCR7-deficient mice. These results strongly suggest that both the R1 and R2 LP-DC subsets migrate to the MLNs in a CCR7-dependent manner under steady-state conditions. Consistent with this, both these LP-DC subsets were present in the intestine of CCR7-deficient mice (M. H. Jang and N. Sougawa, unpublished observation).

We also found that the majority of MLN-DCs were CCR7$^+$, as evidenced by their binding of a CCL19 fusion protein (Fig. 2*B*), and like the unique DCs documented in rat intestinal lymph by Huang et al. (15), MLN-DCs contained much debris in the cytoplasm (Fig. 4*A*). The pieces of debris were TUNEL positive, that is, they showed apoptosis-induced DNA fragmentation (Fig. 4*B*). In addition, a considerable proportion of these cells contained granules that were positive for alkaline phosphatase (Fig. 4*C*), which is expressed in epithelial cells, but not DCs. In contrast, the MLN-DCs themselves showed little phagocytic activity, as described below. These results are compatible with the idea that the CCR7$^+$ MLN-DCs were derived from the LP in a CCR7-dependent manner, after having ingested apoptotic IECs in the LP.

LP-DCs efficiently endocytose apoptotic epithelial cells

Because IECs undergo apoptosis extensively in situ, and because the DCs containing apoptotic epithelial cells are found in mesenteric lymph (15), we examined whether LP-DCs are unique in their ability to take up apoptotic IECs by observing isolated LP-DCs by transmission electron microscopy. As shown in Fig. 4*D*, the cytoplasm of the R1 cells contained numerous inclusions of 1–1.5 μm in diameter with membranous materials inside them, suggesting that these cells have a high phagocytic activity for apoptotic cells. The cytoplasm of the R2 subset contained fewer, but nonetheless distinct, phagocytic vesicles, a conspicuous Golgi network, well-developed rough endoplasmic reticulum, and numerous round mitochondria, suggesting that R2 is less phagocytic, but more active in protein synthesis and secretion, than R1. Both subsets showed a few finger-like protrusions from the cell body, with the protrusions from R2 cells being finer than those from R1 cells. These observations indicate that LP-DCs are highly active in the metabolism and phagocytosis of apoptotic cells.

Consistent with the above findings, in vitro analysis showed that both LP-DC subsets were highly phagocytic, efficiently and vigorously taking up CFSE-labeled apoptotic IECs (Fig. 4*E*), with the R1 subset taking up these cells more avidly than the R2 subset, as evidenced by conspicuous IEC-associated fluorescence staining in the cytoplasm (Fig. 4*F*). PP-DCs were heterogeneous in their phagocytic activity, with the CD11b$^-$ fraction of the population taking up apoptotic cells efficiently, and the CD11b$^+$ population showing less activity. In contrast, the MLN-DCs had little phagocytic activity regardless of their CD11b expression, and CD11b$^-$ SP-DCs showed intermediate levels of phagocytosis.

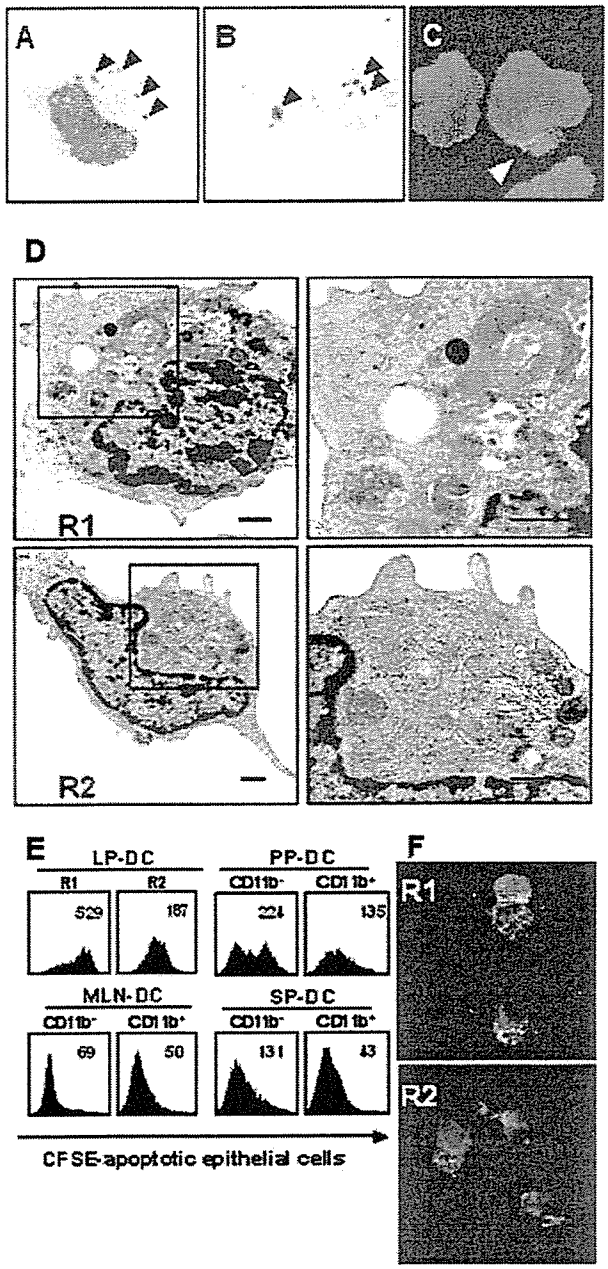

FIGURE 4. LP-DC subsets efficiently endocytose apoptotic IECs. *A–C*, The cytoplasm of MLN-DCs bearing the unique LP-DC phenotype contains cellular debris and fragmented DNA. *A*, FACS-sorted CD11c^{high}CD8$\alpha^{int}\alpha_L{}^{low}\beta_7{}^{high}$ MLN-DC stained with May-Grunwald-Giemsa shows abundant cellular debris in the cytoplasm. *B*, Two CD11c^{high}CD8$\alpha^{int}\alpha_L{}^{low}\beta_7{}^{high}$ MLN-DCs show TUNEL-positive inclusions. *C*, A CD11c^{high}CD8$\alpha^{int}\alpha_L{}^{low}\beta_7{}^{high}$ MLN-DC shows alkaline phosphatase-positive inclusions in the cytoplasm. *D*, Representative transmission electron microscopic views of cells from the LP-DC R1 (*upper*) and R2 (*lower*) subsets. All bars = 1 μm. *E*, Enriched DCs were cocultured with CFSE-labeled apoptotic IECs for 4 h. The DCs were then collected and stained for CD11c and CD11b and analyzed by flow cytometry. The numbers in the histograms indicate the MFI. *F*, Confocal microscopic images showing the uptake of CFSE-labeled apoptotic IECs by LP-DCs.

LP-DCs presenting IEC-associated Ag induce the differentiation of IL-10- and IL-4-producing CD4$^+$ T cells

We next investigated whether LP-DCs could present Ag associated with apoptotic cells to T cells. For this purpose, freshly isolated IECs from the small intestine were intracellularly loaded with OVA by osmotic shock and then allowed to undergo apoptosis spontaneously. Subsequently, the OVA-loaded apoptotic IECs were cocultured with DCs for 4 h, and the Ag-pulsed DC subsets were subjected to cell sorting. The purified DCs were then cocultured with DO11.10 T cells for 6 days, and T cell proliferation was measured by CFSE dilution. As shown in Fig. 5*A*, both the LP-DC subsets induced vigorous T cell proliferation, whereas a subset of SP-DCs, CD11b$^-$ SP-DCs, which displayed moderate phagocytic activity, induced slightly less T cell proliferation than the LP-DCs. The CD11b$^+$ SP-DCs, which had much less phagocytic activity than the LP-DCs, induced only weak proliferation. These results show that LP-DCs can take up apoptotic cells and present cell-associated Ags to T cells more potently than splenic DCs.

Mucosal DCs from the PPs and lungs tend to induce Th2 responses in T cell priming assays (3, 32). We therefore addressed whether LP-DCs also show this tendency by examining the cytokine secretion of OVA TCR-transgenic CD4$^+$ T cells primed by LP-DCs that had been exposed to OVA-loaded apoptotic IECs. As shown in Fig. 5*B*, T cells primed by LP-DCs expressed significantly higher levels of IL-4 and IL-10 than did SP-DC-primed T

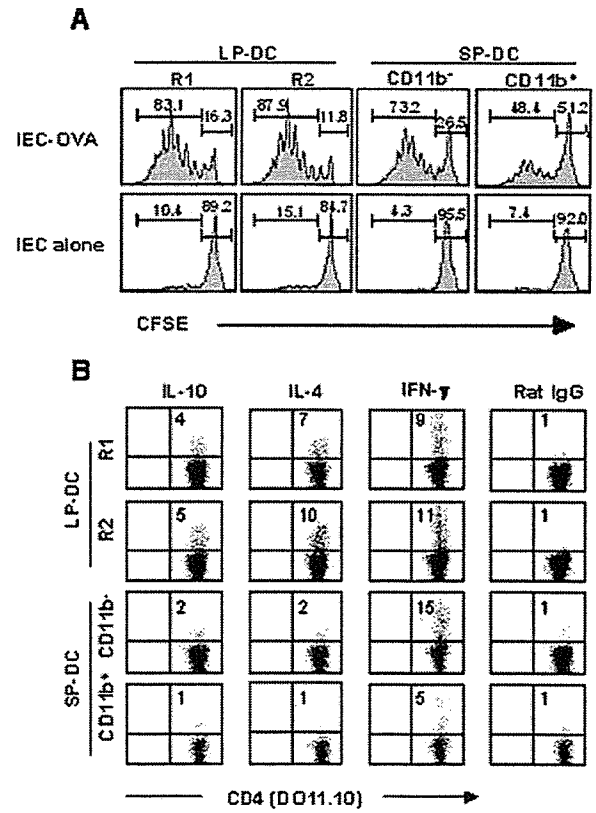

FIGURE 5. LP-DC subsets present IEC-associated Ags. *A*, LP-DC subsets induced cell-associated, Ag-specific T cell proliferation. Freshly isolated IECs were intracellularly loaded with OVA by osmotic shock, then allowed to undergo apoptosis spontaneously. LP-DCs were cocultured with the apoptotic IECs for 4 h, and the DCs were sorted using a FACSVantage SE. Subsequently, purified DCs bearing the OVA-containing IECs were cultured with naive DO11.10 T cells for 6 days. *B*, The LP-DCs primed DO11.10 T cells to produce IL-4 and IL-10. DCs bearing OVA-containing IECs were then cultured with DO11.10 T cells for 14 days (two rounds of stimulation with a 7-day interval). For intracellular cytokine staining, the T cells were restimulated with the anti-CD3ϵ mAb for 6 h in the presence of monensin. The data are representative of three independent experiments. Numbers within a quadrant indicate the percentage of cytokine-producing cells.

cells. The production of IFN-γ was comparable among the T cells primed with the different DCs. These results indicate that LP-DCs have a propensity to induce IL-4- and IL-10-producing T cells when exposed to Ag associated with apoptotic IECs.

Discussion

In this study we showed that there are at least two LP-DC subsets in the intestinal LP of unperturbed mice, and they both require CCR7 for their constitutive migration to MLNs. As speculated previously (15), LP-DCs can, in fact, present Ag associated with apoptotic IECs to naive $CD4^+$ T cells to induce the differentiation of IL-4- and IL-10-producing T cells. These observations indicate that LP-DCs with unique immunomodulatory activities migrate to MLNs in a CCR7-dependent manner to engage in the presentation of IEC-associated Ags from apoptotic IECs that were phagocytosed locally; this may help explain how a noninflammatory immune response can be maintained in MLNs under steady-state conditions.

Although it is generally accepted that DC migration is largely under the control of chemokines and chemokine receptors, studies of the molecules responsible for the migration of LP-DCs to MLNs in the steady state are lacking. The almost complete absence of DCs bearing the LP-DC phenotype ($CD11c^{high}CD8\alpha^{int}\beta_7{}^{high}$ and $CD11c^{high}CD8\alpha^-\beta_7{}^{high}$) in the MLNs of CCR7-deficient mice and their marked reduction in the MLNs of *plt/plt* mice, as shown in this study, provide strong evidence that CCR7 is critically important for LP-DC migration to the MLNs. Our unpublished observation that LP-DCs were found in the intestines of CCR7-deficient mice also supports this hypothesis. The ligands for CCR7 are CCL19 and CCL21. The *plt/plt* mouse strain congenitally lacks the expression of CCL19 and CCL21-Ser, but does express another CCL21 gene product, CCL21-Leu, in lymphatic endothelial cells (20). Thus, our data point to a critical role for CCR7-mediated signaling at the step of DC entry into the intestinal lymphatics, although additional investigation is required to pinpoint the site(s) of action of CCR7-mediated signaling. A pivotal role for CCR7 in the migration of skin DCs to afferent dermal lymphatics has been indicated in a report by Ohl et al. (23).

CCR7-mediated signaling may also play a role in the maturation and survival of LP-DCs transported to the MLNs, because CCR7 has been shown to induce antiapoptotic signaling (33) and terminal activation (34) in DCs. Although this issue could, in theory, be investigated by comparing the fate of CCR7-deficient vs wild-type LP-DCs within MLNs upon their injection into the intestinal lymphatics, a technical difficulty involved in applying this procedure to the mouse has prevented us from performing such experiments.

It is of note that although LP-DCs appeared to be relatively immature, showing a $CD80^{low}CD86^{int}$MHC class $II^{low}CD40^{low}$ phenotype, they expressed CCR7 and functionally responded avidly to CCL21 like mature DCs (19, 35). Given that immature DCs, albeit CCR7 negative initially, up-regulate their CCR7 expression upon ingestion of opsonized apoptotic cells (36), it is tempting to speculate that LP-DCs acquire CCR7 expression through the ingestion of apoptotic IECs in situ.

In contrast to the LP-derived DCs, the number of PP-derived DCs ($CD8\alpha^{high}\beta_7{}^{int}$ and $CD8\alpha^-\beta_7{}^{low}$) was not lower in the MLNs of *plt/plt* and CCR7-deficient mice (Fig. 4), indicating that PP-DCs do not depend on CCR7 signaling for migration to the MLNs. Previous studies showed that different PP-DC subsets differentially express multiple chemokine receptors, including CCR1, CCR2, CCR5, CCR7, CCR9, and CCR10, with all the subsets expressing functional CCR7 (4, 37). Although PP-DCs may use CCR7-mediated signaling for their localization within PP microdomains, as suggested previously (4), our study indicates that PP-DCs depend on non-CCR7 ligand chemokine(s) for their steady-state migration to MLNs.

Although recent studies of murine LP-DCs have identified several distinct subsets, i.e., $CD11c^+CD8\alpha^-CD11b^+$ (14, 38), $CD11c^+CD8\alpha^-CD11b^-$ (11, 14), $CD11c^+CD8\alpha^+CD11b^-$, $CD11c^{int}CD8\alpha^-CD11b^+B220^+$ (14), and $CD11c^-CD11b^-$ (30), our data presented in this paper clearly showed that, among these groups, the major contributors are from two populations, i.e., $CD11c^{high}CD8\alpha^{int}CD11b^{low}\alpha_L{}^{low}\beta_7{}^{high}$ (R1) and $CD11c^{high}CD8\alpha^-CD11b^{high}\alpha_L{}^{low}\beta_7{}^{high}$ (R2), in unperturbed mice. We also observed $CD11c^{int}CD11b^{high}$ cells to be abundant in the LP, but we did not include them in our current analysis, because they appeared to be different from conventional DCs, with numerous cytoplasmic eosinophilic granules. There were also low numbers of DC-like cells in our LP cell population, but they constituted only a very small proportion of the cells compared with R1 and R2, and thus they were not analyzed in the current study.

The recently reported $CD11c^+CD8\alpha^-CD11b^-$ LP-DCs constitutively expressing the IL-12 p40 promoter (11) and APCs with the $CD11c^-CD11b^-$ phenotype that constitutively express CD70 (30) may have been among the cell populations we did not study. In addition, a recent study identified $CX3CR1^+$ LP-DCs that form dendrites through the IECs of the terminal ileum to sample bacteria in the lumen directly (10). Because these $CX3CR1^+$ LP-DCs are $CD11c^{high}CD11b^{high}$, they resemble the R2 subset of our analysis. However, our preliminary observation indicates that hardly any cells in the R2 subset were reactive with an anti-CX_3CR1 mAb (M. H. Jang and N. Sougawa, unpublished observation).

Previous reports by Huang et al. (15) using mesenteric lymphadenectomized rats showed a DC subset in the intestinal lymph that constitutively transports apoptotic IECs to the T cell areas in MLNs. Our study demonstrated that although MLN-DCs with the LP-DC phenotype are poorly phagocytic, there is irrefutable evidence of previous phagocytosis, inasmuch as they contain much intracytoplasmic cellular debris, and both $CD8\alpha^{int}$ and $CD8\alpha^-$ LP-DC subsets can ingest apoptotic IECs vigorously and present IEC-associated Ag to $CD4^+$ T cells in vitro. These results strongly indicate that MLN-DCs containing considerable cellular debris correspond to the cells identified in the intestinal lymph by Huang et al. (15), and that the site of apoptotic cell acquisition by these cells is the LP.

Our observation that LP-DCs could polarize $CD4^+$ T cell differentiation to favor IL-4- and IL-10-producing T cells subsequent to coculture with Ag-loaded apoptotic IECs parallels the observation by Iwasaki and Kelsall (3) that PP-DCs generate T cells that produce high levels of IL-4 and IL-10 and less IFN-γ, as well as the observation by Alpan et al. (39) that Ag-loaded DCs present in MLNs can induce T cells to produce IL-4 and IL-10. Thus, certain intestinal DCs, including the LP-DCs, may have a tendency to induce Th2, rather than Th1, cells, which may be, at least in part, related to their localization to a specific microenvironment. Because phagocytosis of apoptotic cells has been reported to result in an anti-inflammatory state via transcriptional suppression of IL-12 (40), DCs that are closely colocalized with IECs in the LP may become locally imprinted not to induce Th1 cells upon ingestion of apoptotic IECs. In addition, conditioned medium of IECs have been shown to induce DCs to release IL-6 and to prime Th2 responses (41). Thus, the local microenvironment appears to confer on DCs a propensity to induce Th2 cells.

Collectively, these data provide strong evidence that CCR7 is critical for the recruitment of LP-DCs into the MLNs under steady-state conditions. Because these LP-DCs phagocytose apoptotic IECs and present IEC-associated Ag to induce IL-4- and IL-10-producing $CD4^+$ T cells, they are likely to be involved in the

immunomodulation of T cells within the MLNs. Thus, our study strengthens the idea that CCR7 is involved in the maintenance of peripheral tolerance (23) and points to a role for CCR7 in the recruitment of immunomodulatory DCs to the MLNs.

Acknowledgments

We thank Drs. S. Ono, H. Nakano, Y. Takahama, K. Matsushima, K. Hieshima, and O. Yoshie for providing valuable reagents and/or animals, and Dr. H. Hayasaka for critical reading of the manuscript. We also thank S. Yamashita and M. Komine for secretarial assistance, and Y. Nakano for technical help.

Disclosures

The authors have no financial conflict of interest.

References

1. Banchereau, J., F. Briere, C. Caux, J. Davoust, S. Lebecque, Y. J. Liu, B. Pulendran, and K. Palucka. 2000. Immunobiology of dendritic cells. *Annu. Rev. Immunol.* 18: 767–811.
2. Kelsall, B. L., and M. Rescigno. 2004. Mucosal dendritic cells in immunity and inflammation. *Nat. Immunol.* 5: 1091–1095.
3. Iwasaki, A., and B. L. Kelsall. 1999. Freshly isolated Peyer's patch, but not spleen, dendritic cells produce interleukin 10 and induce the differentiation of T helper type 2 cells. *J. Exp. Med.* 190: 229–239.
4. Iwasaki, A., and B. L. Kelsall. 2000. Localization of distinct Peyer's patch dendritic cell subsets and their recruitment by chemokines macrophage inflammatory protein (MIP)-3α, MIP-3β, and secondary lymphoid organ chemokine. *J. Exp. Med.* 191: 1381–1394.
5. Iwasaki, A., and B. L. Kelsall. 2001. Unique functions of CD11b$^+$, CD8α^+, and double-negative Peyer's patch dendritic cells. *J. Immunol.* 166: 4884–4890.
6. Kelsall, B. L., and W. Strober. 1996. Distinct populations of dendritic cells are present in the subepithelial dome and T cell regions of the murine Peyer's patch. *J. Exp. Med.* 183: 237–247.
7. Mora, J. R., M. R. Bono, N. Manjunath, W. Weninger, L. L. Cavanagh, M. Rosemblatt, and U. H. Von Andrian. 2003. Selective imprinting of gut-homing T cells by Peyer's patch dendritic cells. *Nature* 424: 88–93.
8. Iwata, M., A. Hirakiyama, Y. Eshima, H. Kagechika, C. Kato, and S. Y. Song. 2004. Retinoic acid imprints gut-homing specificity on T cells. *Immunity* 21: 527–538.
9. Rescigno, M., M. Urbano, B. Valzasina, M. Francolini, G. Rotta, R. Bonasio, F. Granucci, J. P. Kraehenbuhl, and P. Ricciardi-Castagnoli. 2001. Dendritic cells express tight junction proteins and penetrate gut epithelial monolayers to sample bacteria. *Nat. Immunol.* 2: 361–367.
10. Niess, J. H., S. Brand, X. Gu, L. Landsman, S. Jung, B. A. McCormick, J. M. Vyas, M. Boes, H. L. Ploegh, J. G. Fox, et al. 2005. CX_3CR1-mediated dendritic cell access to the intestinal lumen and bacterial clearance. *Science* 307: 254–258.
11. Becker, C., S. Wirtz, M. Blessing, J. Pirhonen, D. Strand, O. Bechthold, J. Frick, P. R. Galle, I. Autenrieth, and M. F. Neurath. 2003. Constitutive p40 promoter activation and IL-23 production in the terminal ileum mediated by dendritic cells. *J. Clin. Invest.* 112: 693–706.
12. Fagarasan, S., and T. Honjo. 2004. Regulation of IgA synthesis at mucosal surfaces. *Curr. Opin. Immunol.* 16: 277–283.
13. Fagarasan, S., K. Kinoshita, M. Muramatsu, K. Ikuta, and T. Honjo. 2001. In situ class switching and differentiation to IgA-producing cells in the gut lamina propria. *Nature* 413: 639–643.
14. Chirdo, F. G., O. R. Millington, H. Beacock-Sharp, and A. M. Mowat. 2005. Immunomodulatory dendritic cells in intestinal lamina propria. *Eur. J. Immunol.* 35: 1831–1840.
15. Huang, F. P., N. Platt, M. Wykes, J. R. Major, T. J. Powell, C. D. Jenkins, and G. G. MacPherson. 2000. A discrete subpopulation of dendritic cells transports apoptotic intestinal epithelial cells to T cell areas of mesenteric lymph nodes. *J. Exp. Med.* 191: 435–444.
16. Chung, Y., J. H. Chang, M. N. Kweon, P. D. Rennert, and C. Y. Kang. 2005. CD8α^-11b$^+$ dendritic cells but not CD8α^+ dendritic cells mediate cross-tolerance toward intestinal antigens. *Blood* 106: 201–206.
17. Chan, V. W., S. Kothakota, M. C. Rohan, L. Panganiban-Lustan, J. P. Gardner, M. S. Wachowicz, J. A. Winter, and L. T. Williams. 1999. Secondary lymphoid-tissue chemokine (SLC) is chemotactic for mature dendritic cells. *Blood* 93: 3610–3616.
18. Dieu, M. C., B. Vanbervliet, A. Vicari, J. M. Bridon, E. Oldham, S. Ait-Yahia, F. Briere, A. Zlotnik, S. Lebecque, and C. Caux. 1998. Selective recruitment of immature and mature dendritic cells by distinct chemokines expressed in different anatomic sites. *J. Exp. Med.* 188: 373–386.
19. Sallusto, F., P. Schaerli, P. Loetscher, C. Schaniel, D. Lenig, C. R. Mackay, S. Qin, and A. Lanzavecchia. 1998. Rapid and coordinated switch in chemokine receptor expression during dendritic cell maturation. *Eur. J. Immunol.* 28: 2760–2769.
20. von Andrian, U. H., and T. R. Mempel. 2003. Homing and cellular traffic in lymph nodes. *Nat. Rev. Immunol.* 3: 867–878.
21. Forster, R., A. Schubel, D. Breitfeld, E. Kremmer, I. Renner-Muller, E. Wolf, and M. Lipp. 1999. CCR7 coordinates the primary immune response by establishing functional microenvironments in secondary lymphoid organs. *Cell* 99: 23–33.
22. Gunn, M. D., S. Kyuwa, C. Tam, T. Kakiuchi, A. Matsuzawa, L. T. Williams, and H. Nakano. 1999. Mice lacking expression of secondary lymphoid organ chemokine have defects in lymphocyte homing and dendritic cell localization. *J. Exp. Med.* 189: 451–460.
23. Ohl, L., M. Mohaupt, N. Czeloth, G. Hintzen, Z. Kiafard, J. Zwirner, T. Blankenstein, G. Henning, and R. Forster. 2004. CCR7 governs skin dendritic cell migration under inflammatory and steady-state conditions. *Immunity* 21: 279–288.
24. Kellermann, S. A., S. Hudak, E. R. Oldham, Y. J. Liu, and L. M. McEvoy. 1999. The CC chemokine receptor-7 ligands 6Ckine and macrophage inflammatory protein-3β are potent chemoattractants for in vitro- and in vivo-derived dendritic cells. *J. Immunol.* 162: 3859–3864.
25. Kanegasaki, S., Y. Nomura, N. Nitta, S. Akiyama, T. Tamatani, Y. Goshoh, T. Yoshida, T. Sato, and Y. Kikuchi. 2003. A novel optical assay system for the quantitative measurement of chemotaxis. *J. Immunol. Methods* 282: 1–11.
26. Yamamoto, M., K. Fujihashi, K. Kawabata, J. R. McGhee, and H. Kiyono. 1998. A mucosal intranet: intestinal epithelial cells down-regulate intraepithelial, but not peripheral, T lymphocytes. *J. Immunol.* 160: 2188–2196.
27. Haan, J. d., S. Lehar, and M. Bevan. 2000. CD8$^+$ but not CD8$^-$ dendritic cells cross-prime cytotoxic T cells in vivo. *J. Exp. Med.* 192: 1685–1696.
28. Yokota, Y., A. Mansouri, S. Mori, S. Sugawara, S. Adachi, S. Nishikawa, and P. Gruss. 1999. Development of peripheral lymphoid organs and natural killer cells depends on the helix-loop-helix inhibitor Id2. *Nature* 397: 702–706.
29. Nakano, H., M. Yanagita, and M. D. Gunn. 2001. CD11c$^+$B220$^+$Gr-1$^+$ cells in mouse lymph nodes and spleen display characteristics of plasmacytoid dendritic cells. *J. Exp. Med.* 194: 1171–1178.
30. Laouar, A., V. Haridas, D. Vargas, X. Zhinan, D. Chaplin, R. A. van Lier, and N. Manjunath. 2005. CD70$^+$ antigen-presenting cells control the proliferation and differentiation of T cells in the intestinal mucosa. *Nat. Immunol.* 6: 698–706.
31. Ardavin, C. 2003. Origin, precursors and differentiation of mouse dendritic cells. *Nat. Rev. Immunol.* 3: 582–590.
32. Akbari, O., R. H. DeKruyff, and D. T. Umetsu. 2001. Pulmonary dendritic cells producing IL-10 mediate tolerance induced by respiratory exposure to antigen. *Nat. Immunol.* 2: 725–731.
33. Sanchez-Sanchez, N., L. Riol-Blanco, G. de la Rosa, A. Puig-Kroger, J. Garcia-Bordas, D. Martin, N. Longo, A. Cuadrado, C. Cabanas, A. L. Corbi, et al. 2004. Chemokine receptor CCR7 induces intracellular signaling that inhibits apoptosis of mature dendritic cells. *Blood* 104: 619–625.
34. Marsland, B. J., P. Battig, M. Bauer, C. Ruedl, U. Lassing, R. R. Beerli, K. Dietmeier, L. Ivanova, T. Pfister, L. Vogt, et al. 2005. CCL19 and CCL21 induce a potent proinflammatory differentiation program in licensed dendritic cells. *Immunity* 22: 493–505.
35. Yanagihara, S., E. Komura, J. Nagafune, H. Watarai, and Y. Yamaguchi. 1998. EBI1/CCR7 is a new member of dendritic cell chemokine receptor that is up-regulated upon maturation. *J. Immunol.* 161: 3096–3102.
36. Verbovetski, I., H. Bychkov, U. Trahtemberg, I. Shapira, M. Hareuveni, O. Ben-Tal, I. Kutikov, O. Gill, and D. Mevorach. 2002. Opsonization of apoptotic cells by autologous iC3b facilitates clearance by immature dendritic cells, down-regulates DR and CD86, and up-regulates CC chemokine receptor 7. *J. Exp. Med.* 196: 1553–1561.
37. Zhao, X., A. Sato, C. S. Dela Cruz, M. Linehan, A. Luegering, T. Kucharzik, A. K. Shirakawa, G. Marquez, J. M. Farber, I. Williams, et al. 2003. CCL9 is secreted by the follicle-associated epithelium and recruits dome region Peyer's patch CD11b$^+$ dendritic cells. *J. Immunol.* 171: 2797–2803.
38. Anjuere, F., C. Luci, M. Lebens, D. Rousseau, C. Hervouet, G. Milon, J. Holmgren, C. Ardavin, and C. Czerkinsky. 2004. In vivo adjuvant-induced mobilization and maturation of gut dendritic cells after oral administration of cholera toxin. *J. Immunol.* 173: 5103–5111.
39. Alpan, O., G. Rudomen, and P. Matzinger. 2001. The role of dendritic cells, B cells, and M cells in gut-oriented immune responses. *J. Immunol.* 166: 4843–4852.
40. Kim, S., K. B. Elkon, and X. Ma. 2004. Transcriptional suppression of interleukin-12 gene expression following phagocytosis of apoptotic cells. *Immunity* 21: 643–653.
41. Rimoldi, M., M. Chieppa, V. Salucci, F. Avogadri, A. Sonzogni, G. M. Sampietro, A. Nespoli, G. Viale, P. Allavena, and M. Rescigno. 2005. Intestinal immune homeostasis is regulated by the crosstalk between epithelial cells and dendritic cells. *Nat. Immunol.* 6: 507–514.

Available online at www.sciencedirect.com
SCIENCE DIRECT®
Developmental and Comparative Immunology 30 (2006) 667–683
Developmental & Comparative Immunology
www.elsevier.com/locate/devcompimm

Differences in integrin-dependent phagocytosis among three hemocyte subpopulations of the Pacific oyster "*Crassostrea gigas*"☆

Kazutaka Terahara [a,b,1,*], Keisuke G. Takahashi [a,d,1], Akifumi Nakamura [a], Makoto Osada [c,d], Masaki Yoda [a,b], Takachika Hiroi [b], Masatomo Hirasawa [e], Katsuyoshi Mori [a,d]

[a] *Laboratory of Aquacultural Biology, Graduate School of Agricultural Science, Tohoku University, Aoba-ku, Sendai, Miyagi 981-8555, Japan*
[b] *Division of Mucosal Immunology, Institute of Medical Science, The University of Tokyo, 4-6-1 Shirokanedai, Minato-ku, Tokyo 108-8639, Japan*
[c] *Laboratory of Ecological Genetics, Graduate School of Agricultural Science, Tohoku University, Onagawa, Oshika 986-2242, Japan*
[d] *Oyster Research Institute, Izumi-ku, Sendai, Miyagi 981-3212, Japan*
[e] *Department of Microbiology, Nihon University School of Dentistry at Matsudo, Matsudo, Chiba, 271-0061, Japan*

Received 9 March 2005; received in revised form 16 September 2005; accepted 26 September 2005
Available online 24 October 2005

Abstract

Integrins play a key role in immunoresponses such as attachment, spreading, and phagocytosis in invertebrate hemocytes. This study was designed to identify integrin expression patterns at the hemocyte subpopulation level, and correlate the expression levels with phagocytic ability. First, we cloned a β integrin from *Crassostrea gigas* hemocytes and used real-time RT-PCR to analyze the quantitative expression level of its encoding mRNA. The expression level in hyalinocytes was significantly higher than that in granulocytes and agranulocytes. Subsequently, we investigated the phagocytic ability of each subpopulation using anti-$\alpha_5\beta_1$ integrin antibody, and found that phagocytosis of hyalinocytes was inhibited by neutralization with the antibody but enhanced against the antibody-conjugated microspheres. In contrast, phagocytic abilities of granulocytes and agranulocytes showed high and zero levels, respectively, regardless of the antibody. These results suggest that phagocytosis of hyalinocytes is regulated by an integrin-dependent mechanism and that of granulocytes is elicited by other functional receptors.
© 2005 Elsevier Ltd. All rights reserved.

Keywords: Bivalve; Cloning; *Crassostrea gigas*; Hemocyte; Integrin; Pacific oyster; Phagocytosis; Real-time RT-PCR

Abbreviations: AAP, abridged anchor primer; AUAP, abridged universal amplification primer; BSS, balanced salt solution; DIG, digoxigenin; EGF, epidermal growth factor; GAPDH, glyceraldehyde 3-phosphate dehydrogenase; GST, glutathione-*S*-transferase; LBD, ligand-binding domain; MIDAS, metal ion-dependent adhesion site; ORF, open reading frame; PI, phagocytic index; PR, phagocytic rate; RACE, rapid amplification of cDNA ends; RGD, Arg-Gly-Asp; RT-PCR, reverse transcription-polymerase chain reaction; SD, standard deviation; SDS-PAGE, sodium dodecyl sulfate polyacrylamide gel electrophoresis; SE, standard error; ss cDNA, single strand cDNA.

☆ The nucleotide sequence reported was submitted to GenBank and is available under accession number AB066348.

* Corresponding author. Address: Division of Mucosal Immunology, Institute of Medical Science, The University of Tokyo, 4-6-1 Shirokanedai, Minato-ku, Tokyo 108-8639, Japan. Tel.: +81 3 5449 5271; fax: +81 3 5449 5411.
E-mail address: tera@ims.u-tokyo.ac.jp (K. Terahara).

[1] These authors contributed equally to this work.

0145-305X/$ - see front matter © 2005 Elsevier Ltd. All rights reserved.
doi:10.1016/j.dci.2005.09.009

1. Introduction

Integrins belong to a family of transmembrane receptors and consist of non-covalently associated αβ heterodimers, which are divided into three domains: large extracellular, transmembrane, and short cytoplasmic domains [1]. In vertebrates, the functional importance of integrins in the regulation of cell adhesion, migration, proliferation, and apoptosis through transmission from the outer environment into the cytoplasm is well known [1–3]. Invertebrate integrins are also responsible for cellular adhesive processes correlated with several immune responses [4]. For example, experiments using Arg-Gly-Asp (RGD)-containing peptides as a competitor of integrin-ligand binding have demonstrated that RGD-recognizing integrins or integrin-like molecules are involved in adhesion (or spreading) [5–7], degranulation [8], phagocytosis [7,9], and encapsulation [10]. In addition to the above experiments using RGD peptides, an anti-integrin antibody has been used to demonstrate that the integrin of ascidian hemocytes is involved in C3-dependent phagocytosis [11].

In bivalve molluscs, as well as other invertebrates, circulating hemocytes play a crucial role in innate immune responses such as phagocytosis, inflammation, and wound repair, which modulate host defense mechanisms and homeostasis [12,13]. Referring to the information from other invertebrates described above, it can be considered that these cellular immune responses of bivalve hemocytes are also modulated by specific membrane receptors such as integrins for transmission of suitable signals into the cytoplasm. During our studies on the functional role of putative integrins in hemocyte responses in the Pacific oyster *Crassostrea gigas*, a bivalve molluscan species, we found that the spreading ability of hemocytes was reduced and simultaneously apoptosis was induced by treatment with RGD peptides [14,15]. Further, we found that adhesion and spreading abilities of *C. gigas* hemocytes were enhanced by immobilized ligands containing the RGD motif and by divalent cations, and that the spreading hemocytes then underwent apoptosis at least 24 h later regardless of treatment with free RGD peptides [16]. These previous findings indicate that *C. gigas* hemocytes possess potential integrins, which function during hemocyte-adhesion and induction of apoptosis dependent on RGD-recognition. However, to date, integrins from *C. gigas* hemocytes as well as other bivalve cells have not been identified at protein or gene levels.

Bivalve hemocytes comprise various subpopulations that express different forms and functions, as with other invertebrate hemocytes [12,17,18]. Although functional analyses of integrins have been performed in hemocytes of many invertebrate species, such analyses have not been undertaken at a hemocyte subpopulation level, aside from one study on ascidian hemocytes [19]. Ascidian β integrin (β_{Hr1}) was shown to be expressed more remarkably in phago-amoebocytes and lymphoid cells than in fusogenic phagocytes and vacuolated cells by immunocytochemical staining with anti-β_{Hr1} antiserum [19]. Elucidation of the different expression patterns of an integrin gene and its related cellular responses would be helpful in understanding the immuno-functions of each hemocyte subpopulation. To this end, this study aimed to compare levels of integrin-related immuno-functions such as phagocytosis among *C. gigas* hemocyte subpopulations.

2. Materials and methods

2.1. Oysters

Two-year-old Pacific oysters, *C. gigas*, were obtained from a hanging culture bed in Matsushima Bay, Miyagi Prefecture, Japan, from 2000 to 2005. They were transferred to our laboratory and maintained in 150-l aquariums with recirculating, filtered artificial seawater (MARINE ART BR, Senju Seiyaku Co., Osaka, Japan) at 15 °C until use.

2.2. Primers for polymerase chain reaction (PCR)

All of the designed primers were produced by Nihon Gene Research Laboratories, Sendai, Japan. Primer sequences are listed in Table 1.

2.3. Preparation of total RNA, mRNA, and single strand cDNA from C. gigas hemocytes

Hemolymph samples were obtained from the adductor muscle using a plastic syringe with a 25-gauge, 1.0-in. long needle and centrifuged at 500 *g* for 15 min at 4 °C. The resulting pellet was lyzed with ISOGEN (Nippon Gene Co. Ltd, Toyama, Japan) for isolation of total RNA. Messenger RNA was separated from the total RNA using an Oligotex-dT30 <Super> Kit (Roche Diagnostics, Mannheim, Germany) and then reverse-transcribed using a first Strand cDNA Synthesis Kit for RT-PCR (AMV) (Roche Diagnostics) with an oligo-dT primer (Roche Diagnostics) to generate single strand (ss) cDNA as a template for PCR.

Table 1
Sequences of PCR primers

Experiment	Primer	Sequence	Position in *C. gigas* β integrin
Cloning	F1	5′-TACTA(CT)TTGATGGATCTCTC-3′	457–476
	F2	5′-G(AC)AA(CT)TTGGATGCTCC(CG)GAA-3′	740–759
	F3	5′-GAAGACATGAGCACCATCAC-3′	532–551
	F4	5′-GRAACCTTGATGCTTGTG-3′	777–796
	F6	5′-GAAGCTCATGTGTCAGTGTGACTG-3′	1386–1409
	R1	5′-A(CT)(AG)AA(CT)GAACCGAA(AT)CC(AT)-3′	566–583
	R2	5′-A(CT)(AG)AA(CT)GAACCGAA(AT)CC(AT)-3′	842–859
	R3	5′-CACAAGCTATGGCCTGCATG-3′	777–796
	R4	5′-GTGATGGTGCTCATGTCTTC-3′	532–551
	R5	5′-AFCTATCTTGACTCCAAGGC-3′	512–531
	R6	5′-CTTTGTCGTCTGCCATTGGC-3′	480–499
	R7	5′-CATTGGTTCTGTTACACAGCGC-3′	1972–1993
Real-time RT-PCR	F7	5′-TGAGTGTGGCAAGTGTACCT-3′	1869–1888
	F8	5′-GTTATCCCAGATTTGAACGG-3′	
	R8	5′-TATGGGAGCACTCTTTTTCA-3′	2019–2038
	R9	5′-ATCATCTTCTGTGTATCCCA-3′	

The position refers to the nucleotide number in Fig. 2A. A, adenine; C, cytosine; G, guanine; and T, thymine. F1-6 and R1-7 were used for cloning of *C. gigas* β integrin. F7, F8, R8 and R9 were used for real-time RT-PCR. F7 and R8 are primers for *C. gigas* β integrin. F8 and R9 are primers for *C. gigas* GAPDH

2.4. Cloning of *C. gigas* β integrin cDNA

Cloning was performed using a combination of reverse transcription (RT)-polymerase chain reaction (PCR), degenerate PCR, 5′ rapid amplification of cDNA ends (RACE) and 3′ RACE (Fig. 1) on a thermocycler (Model TP2000; Takara, Shiga, Japan) under the PCR programs shown in Table 2. For sequencing, each PCR product was prepared as a template by electrophoresing on agarose gel, then isolated from the gel and subcloned into a TA vector (pCR II; Invitrogen).

Degenerate PCR was initially performed to reveal the partial sequence of the *C. gigas* β integrin with degenerate primers (F1 and R1, or F2 and R2) designed from highly conserved extracellular regions in various invertebrate β integrins and AmpliTaq Gold (Perkin Elmer, Foster City, CA, USA) under PCR program Nos. 1 and 2 (Table 2); fragments 1 and 2 were then obtained (Fig. 1). Furthermore, RT-PCR was performed to amplify the fragment between fragments 1 and 2 with the exact primers F3 and R3 and AmpliTaq Gold under PCR program No. 3 (Table 2); fragment 3 was then obtained (Fig. 1).

5′ RACE technique with a nested PCR was performed to determine the upstream cDNA sequence of fragment 1 using the 5′ RACE System for Rapid Amplification of cDNA Ends, Version 2.0 (Invitrogen). Initially, ss cDNA was prepared as a template from total RNA with primer R4. RT-PCR was subsequently performed with the ss cDNA, primer R5, abridged anchor primer (AAP; Invitrogen) and AmpliTaq Gold under PCR program No. 4 (Table 2). Subsequently, a nested PCR was performed using the above PCR product (approximately 650 bp) as a template, nested primer R6, abridged universal amplification primer (AUAP; Invitrogen) and AmpliTaq Gold under PCR program No. 5 (Table 2); fragment 4 was then obtained (Fig. 1).

3′ RACE technique with two cycles of a nested PCR was performed to determine the downstream cDNA sequence of fragment 2. Initially, ss cDNA was generated as a template from total RNA with a 3′ RACE adaptor primer (Invitrogen) using a First Strand cDNA Synthesis Kit for RT-PCR (Invitrogen). RT-PCR was then performed with the ss cDNA, primers F3 and AUAP, and TaKaRa LA Taq (Takara) under PCR program No. 6 (Table 2). Nested PCR was then performed with the RT-PCR products, nested primer

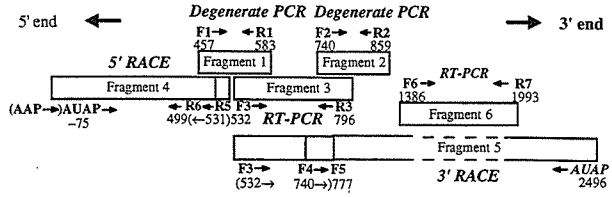

Fig. 1. Schematic diagram of the procedures combined with degenerate PCR, RT-PCR, 5′ RACE, and 3′ RACE methods for cloning *C. gigas* β integrin. Numbers represent nucleotide positions in Fig. 2A.

Table 2
PCR conditions for cloning of *C. gigas* β integrin

PCR no.	PCR method (fragment)	Primer	Pre-healing	Denaturation	Annealing	Extention	Cycles
1	Degenerate PCR (fragment 1)	F1,R1,	94 °C, 9 min	94 °C, 30 s	37 °C, 30 s	72 °C, 30 s	40
2	Degenerate PCR (fragment 2)	F2,R2	94 °C, 9 min	94 °C, 30 s	37 °C, 30 s	72 °C, 30 s	40
3	General RT-PCR (fragment 3)	F3,R3	94 °C, 9 min	94 °C, 1 min	55 °C, 1 min	72 °C, 1 min	35
4	5′RACE; General RT-PCR	AAP, R5	94 °C, 9 min	94 °C, 1 min	55 °C, 1 min	72 °C, 1.5 min	35
5	5′RACE; (fragment 4)	AUAP, R6	94 °C, 9 min	94 °C, 1 min	55 °C, 1 min	72 °C, 1.5 min	35
6	3′RACE; General RT-PCR	F3, AUAP	–	95 °C, 1 min	57 °C, 1.5 min	72 °C, 6 min	40
7	3′RACE; 1st PCR	F4, AUAP	–	94 °C, 1 min	57 °C, 1.5 min	72 °C, 6 min	40
8	3′RACE; 2nd nested PCR (fragment 5)	F5m AUAP	–	94 °C, 1 min	58 °C, 1 min	72 °C, 1.5 min	35
9	General RT-PCR (fragment 6)	F6, R7	94 °C, 9 min	94 °C, 30 s	60 °C, 1 min	72 °C, 1 min	40

F4, AUAP, and TaKaRa LA Taq under PCR program No. 7 (Table 2). A second cycle of nested PCR was performed with the first cycle of nested PCR products, nested primer F5, AUAP and TaKaRa LA Taq under PCR program No. 8 (Table 2); fragment 5 was then obtained (Fig. 1). Because fragment 5 was too long, RT-PCR was performed to reveal the unsequenced region with the ss cDNA, F6 and R7 primers, and AmpliTaq Gold under PCR program No. 9 (Table 2); fragment 6 was then obtained (Fig. 1).

2.5. Northern blot analysis

Digoxigenin (DIG)-labeled fragment 3 was prepared with a PCR DIG Probe Synthesis Kit (Roche Diagnostics). As a positive control, DIG-labeled *C. gigas* glyceraldehyde 3-phosphate dehydrogenase (GAPDH) (GenBank accession No. AJ544886) fragment was prepared using sense primer (F8) and antisense primer (R9). Subsequently, 20 μg of mRNA was denatured with formamide, separated on denaturing 1% agarose gel, transferred to a nylon membrane using a Model 785 Vacuum Blotter (Bio-Rad Laboratories Inc., Hercules, CA, USA), and UV cross-linked to a nylon membrane using a GS Gene Linker UV Chamber (Bio-Rad). The membrane was prehybridized with hybridization buffer (5×SSC, 10×Denhardt's solution, 0.5% SDS, 50% formamide, 0.1 mg/ml denatured salmon sperm DNA) at 50 °C for 3 h in a Model 2000 Hybridization Incubator (Robbins Scientific Co., Sunnyvale, CA, USA), and subsequently hybridized with DIG-labeled cDNA probes dissolved in hybridization buffer at 50 °C for 17 h. The hybridized membrane was washed once with 2×SSC/0.1% SDS at room temperature for 10 min, and twice with 0.2× SSC/0.1% SDS at 55 °C for 20 min. The hybridized probes were then visualized with a DIG Nucleic Acid Detection Kit (Roche Diagnostics).

2.6. Preparation of hemocyte subpopulations by a cell-sorter for quantitative gene expression analysis

Hemocytes from *C. gigas* were divided into three subpopulations: granulocytes, hyalinocytes, and agranulocytes according to their size and complexity using flow cytometry [20,21]. We then applied a cell-sorting system for the preparation of hemocyte subpopulations. Hemolymph samples were subjected to flow cytometric analysis; then each subpopulation was visualized using density plots of forward scatter vs. side scatter, and sorted using FACSAria (Becton Dickinson, San Jose, CA, USA). Parts of each sorted fraction were subjected to flow cytometry to check their purity using FACSDiVa software (Becton Dickinson). Granulocytes, hyalinocytes, and agranulocytes were isolated at 70–75, 80–85, and 90–95% purity, respectively.

2.7. Quantitative real-time RT-PCR for measurements of C. gigas β integrin mRNA levels among hemocyte subpopulations

Quantitative real-time RT-PCR was adopted to measure the expression levels of *C. gigas* β integrin mRNA from freshly sorted hemocyte subpopulations. The expression level of GAPDH mRNA was also analyzed to serve as an internal constitutive marker and to normalize the expression levels of *C. gigas* β integrin mRNA. Total RNAs were extracted from the sorted fractions by TRIzol (Invitrogen). Real-time RT-PCR was performed using hybridization probes on a LightCycler (Roche Diagnostics) [22]. Oligonucleotide primers for *C. gigas* β integrin (F7 and R8), and for

GAPDH (F8 and R9) and hybrid probes for *C. gigas* β integrin (5′-ACTGTGGCCAGGAGCAATGTCG-TACCCACC-3′-FITC and LC Red 640-5′-GGACTG TGCGCTGTGTAACAGAACCAATGCCG-3′) and for GAPDH (5′-TAAAGGGGCATCATACAATGA-TATTAAGGCAGCCA-3′-FITC and LC Red 640-5′-CAAGGCAGCCTCTGAGAATGAATTGAAAGG-3′) were designed and produced by Nihon Gene Research Laboratories. Beforehand, as an external control to obtain a standard curve, RT-PCR products of *C. gigas* β integrin and GAPDH were prepared to be used as templates for real-time RT-PCR with ss cDNA solution, primers F7and R8 for *C. gigas* β integrin (or F8 and R9 for GAPDH), and AmpliTaq Gold. The RT-PCR procedure was as follows: pre-heating at 94 °C for 9 min, 40 cycles of denaturation at 94 °C for 30 s, annealing at 52 °C for 30 s, and extension at 72 °C for 30 s. For amplification of cDNA by real-time RT-PCR, a real-time RT-PCR mixture (20 μl total volume) was prepared as follows: 2 μl of template suspension (total RNA solution from each sorted hemocyte subpopulation or a serial dilution of each *C. gigas* β integrin or GAPDH cDNA), 0.5 μM F7 and R8 (or F8 and R9), 0.2 μM FITC-labeled probe and LC Red 640-labeled probe, 3.25 mM $Mn(OAc)_2$ (Roche Diagnostics), and 1×LightCycler RNA Master Hybridization Probes (Roche Diagnostics). Real-time RT-PCR procedure for *C. gigas* β integrin and GAPDH was performed as follows: RT at 52 °C for 20 min, denaturation at 95 °C for 30 s, 40 cycles of amplification at 95 °C for 1 s, 52 °C for 15 s, and 72 °C for 13 s, and cooling at 40 °C for 30 s. After completion of real-time RT-PCR, the concentrations of target molecules (*C. gigas* β integrin and GAPDH mRNAs) contained in the applied total RNA were calculated with LightCycler Software ver. 3.2 (Roche Diagnostics) and expression levels of *C. gigas* β integrin mRNA were normalized with that of GAPDH mRNA.

2.8. Immunocytochemistry

Hemocyte suspensions in balanced salt solution for *C. gigas* hemocytes (oyster BSS: 446.6 mM NaCl, 14.5 mM KCl, 14.2 mM $MgSO_4$, 10.6 mM $MgCl_2$, 8.6 mM $CaCl_2$, 3.0 mM $NaHCO_3$, 0.08 mM NaH_2PO_4, and 5.6 mM glucose, pH 7.8) [11] were cytospun on glass slides at 60 *g* for 1 min at 4 °C. Cytospin specimens were then fixed in 1.6% formaldehyde neutral buffer solution with PBS (pH 7.4) for 15 min on ice and washed three times with PBS. Cytospin specimens were incubated with goat anti-fibronectin receptor (integrin $\alpha_5\beta_1$) polyclonal antibodies (Chemicon, CA, USA.), which recognize the extracellular domain of integrin $\alpha_5\beta_1$, or normal goat IgG (DakoCytomation) diluted 1/100 in PBS for 1 h at room temperature. After incubation, cytospin specimens were washed three times with PBS and incubated with polyclonal rabbit anti-goat immunoglobulins/FITC-labeled (DakoCytomation, Glostrup, Denmark) diluted 1/200 in PBS for 1 h at room temperature. After incubation, cytospin specimens were washed three times with PBS and observed under a fluorescence microscope.

2.9. Sodium dodecyl sulfate-polyacrylamide gel electrophoresis (SDS-PAGE) and Western blot analysis

Hemolymph was placed onto a plastic culture dish to prepare adherent hemocytes as previously described [14, 15]. Non-adherent hemocytes were removed by washing with oyster BSS while adherent hemocytes were lyzed in SDS-PAGE reducing buffer (0.5 M Tris, 10% SDS, 6% 2-mercaptoethanol, 10% glycerol, and 0.004% bromophenol blue; pH 6.8) and boiled for 5 min. Samples were loaded onto 4-12% Bis-Tris gels (Invitrogen) and separated electrophoretically. After SDS-PAGE, proteins were electro-blotted onto nitrocellulose membranes using a semi-dry transfer unit. Membranes were blocked with 3% non-fat-dry milk in PBS for 1 h at room temperature. After blocking, membranes were incubated at 4 °C overnight with goat anti- integrin $\alpha_5\beta_1$ or rabbit anti-integrin β_1 (Chemicon) polyclonal antibodies diluted 1/200 and 1/500 in PBS, respectively. Normal goat and rabbit sera were also used as negative controls for anti-integrin $\alpha_5\beta_1$ and anti-integrin β_1, respectively. Membranes were then washed three times with 0.1% Tween 20 in PBS, and incubated with alkaline phosphatase (AP)-conjugated donkey anti-goat IgG (Promega, WI, USA) or AP-conjugated goat anti-rabbit IgG (H+L) (Zymed Labotarories Inc., CA, USA) diluted 1/5000 and 1/3000 in PBS, respectively, for 2 h at room temperature. After washing three times with 0.1% Tween 20 in PBS, signals were developed using a BCIP/NBT color development substrate (Promega).

2.10. Phagocytosis assay

To characterize the phagocytic ability of hemocyte subpopulations categorized by flow cytometric analysis, we performed phagocytosis assay according to Takahashi and Mori [23]. In brief, a hemocyte suspension in oyster BSS (5×10^5 cells) was mounted onto glass slides in a moist chamber and

incubated for 30 min at 20 °C. After incubation, hemocyte monolayers were washed three times with oyster BSS and subsequently pre-incubated with the anti-integrin $\alpha_5\beta_1$ antibody diluted 1/100 in oyster BSS for 1 h prior to the addition of zymosan particles (1×10^7 particles/well) suspended with oyster BSS. The other hemocyte monolayers were also pre-incubated with normal goat IgG diluted 1/100 in oyster BSS or only oyster BSS as negative controls. After incubation with zymosan particles for 30 min at 20 °C, the excess particles were removed by washing with oyster BSS, hemocytes were fixed in absolute methanol and May-Grünwald and Giemsa staining was carried out. To estimate the phagocytic ability, we calculated the phagocytic rate (PR) and phagocytic index (PI) by randomly counting a combined total of 500 phagocytic and non-phagocytic hemocyte subpopulations from each monolayer under a light microscope according to Ishikawa et al. [24]. PR and PI were calculated as follows: PR= number of phagocytic hemocytes/total number of hemocytes, PI=number of particles ingested by hemocytes/number of phagocytic hemocytes. In counting, we defined particles engulfed into phagosome of hemocytes as ingested particles.

Further, we also examined the phagocytic ability against anti-integrin $\alpha_5\beta_1$ antibody-conjugated microspheres by *C. gigas* hemocytes. Carboxylated microspheres (ϕ 2.0 μm, Polysciences Inc., Warrington, PA) were covalently coupled with the anti-integrin $\alpha_5\beta_1$ antibody using a Carbodiimide Kit for carboxylated microparticles (Polysciences). Normal goat IgG was also coupled with the carboxylated microspheres as a negative control. Microspheres treated with only oyster BSS were used as another negative control. The antibody-conjugated microspheres were incubated with hemocyte monolayers for 30 min at 20 °C. PR and PI against the microspheres were calculated as described above.

2.11. Statistical analysis

Data were analyzed with one-way ANOVA. Subsequently Tukey's multiple comparison test or Neuman–Keuls multiple comparison test were adopted to test whether the mean values of each experimental group were significantly different, utilizing GraphPad Prism version 4.0 (GraphPad Software Inc., San Diego, CA, USA). Significance was set at $p<0.05$.

3. Results

3.1. Cloning and characterization of C. gigas β integrin cDNA

By assembling the fragments generated by degenerate PCR, RT-PCR, and 5′ and 3′ RACE (Fig. 1), the full sequence of the open reading frame (ORF) (2400 bp, encoding 799 amino acids) of β integrin from *C. gigas* hemocytes was revealed (Fig. 2A). We designated the sequenced β integrin as β_{CGH}.

When β_{CGH} was analyzed in silico, the molecular structure and existence of some functional patterns were revealed. The locations of each domain and their motifs are shown in Fig. 2B. The signal sequence region was assumed to be 17 amino acids long from the N-terminus by signal sequence recognition [25]. Since putative mature β_{CGH} was regarded as being 782 amino acids long, the molecular mass was predicted to be 86,842.94 based on the amino acid content. In addition, eight potential N-glycosylation sites and one tyrosine kinase phosphorylation site were located in the PROSITE database [26]. Therefore, mature β_{CGH} had a predicted molecular mass of 10,6842.94 if 20,000 Da was added to account for the eight potential N-glycosylation sites (2500 Da per N-glycosylation site) because 110,000 Da of human β_1 integrin possessing 12 potential N-glycosylation sites was reduced to 80,000 Da by treatment with N-glycanase [27]. The molecular mass of 106,842.94 Da is consistent with that of other known β subunits (90–110 kDa) [1]. The isoelectric point of the putative mature β_{CGH} was determined as 5.04. The putative transmembrane domain was assumed to be located from the 732nd to 754th amino acid residues using SOSUI [28]; therefore, it was predicted that the putative mature β_{CGH} was composed of one each of extracellular, transmembrane, and cytoplasmic domains with 714, 23, and 45 amino acids, respectively. The ligand-binding domain (LBD) was predicted in the extracellular domain according to the consensus sequence of β integrin LBD [29]. A metal ion-dependent adhesion site (MIDAS) with a DXSXS motif, which is thought to be involved in coordination of divalent cations for ligand binding [30,31], existed in the LBD. An abundance of cysteine residues has also been characterized as a feature of β integrins [1]. There were 58 cysteine residues in the extracellular domain of β_{CGH} (Fig. 3). Two homologous cysteine-rich repeat signatures (consensus: CX[GNQ]X(1,3)GXCXCX(2) CXC) [29] were found in the extracellular domain. Furthermore, using the PROSITE database, two epidermal growth factor (EGF)-like domain signature 1 sequences (consensus:

CXCX(5)GX(2)C) and two EGF-like domain signature 2 sequences (consensus: CXCX(2)[GP][FYW]X(4,8) C), which were equal to or overlapping with the EGF-like domain signature 1 sequences, were found in the extracellular domain. In the cytoplasmic domain, two NPXY motifs, thought to be involved in activating integrins by inducing conformational changes [32,33], were found; as were two protein kinase C (PKC) phosphorylation sites (consensus: [ST]X[RK]). The membrane proximal region motif (LlviXhDR; less conserved amino acids are in lower case), which is thought to regulate the binding affinity states of integrins

A

```
                                tcaccaacaaaagtgttctcttatcgttgattcgccgttaatgtaattttgattgtacagttgctggagaaaga  -1
   ATGGTATCGACGGTTTGGTTTTTATGTTTTACAACAATTTTCTGTTCCCTAAATCCTATCGGGAAATTGAGTGCACAAGATTTACGATCT   90
 1 M  V  S  T  V  W  F  L  C  F  T  T  I  F  C  S  L  N  P  I  G  K  L  S  A  Q  D  L  R  S
   GATACTTTGACGCCTACACAGGAAAACCCGTGCCTGAAGGAAAAGACCACAACATGTGGGGAGTGTATAGCAATATCTACCCTGTGTGCA  180
31 D  T  L  T  P  T  Q  E  N  P  C  L  K  E  K  T  T  T  C  G  E  C  I  A  I  S  T  L  C  A
   TTCTGTACCGACGCTGAGTATGACGCCAACAATTATCCCAGGTGTGACCTACTGACCACTCATCAGAAACTCATCAACAACAAGCCCAGG  270
61 F  C  T  D  A  E  Y  D  A  N  N  Y  P  R  C  D  L  L  T  T  H  Q  K  L  I  N  N  K  P  R
   TGTAAAGACATCGTCAATCCGTCATCAACCCTCGTAAAGAGCAGGGATGACAGATTGATTGATGGCGATAGGGACAGATATGCCGTACAG  360
91 C  K  D  I  V  N  P  S  S  T  L  V  K  S  R  D  D  R  L  I  D  G  D  R  D  R  Y  A  V  Q
   ATCAGACCCCAGCAAATCGACCTGGAGTTACGTCCAAATGACCCTCAGACATTTAATCTGACGTTCCGATTGGCTGAGAACTATCCAGTC  450
121 I  R  P  Q  Q  I  D  L  E  L  R  P  N  D  P  Q  T  F  N* L  T  F  R  L  A  E  N  Y  P  V
   GACCTCTACTACCTTATGGACCTCTCAAACTCCATGGCAGACGACAAAGAAAAACTGGCCAGCCTTGGAGTCAAGATAGCTGAAGACATG  540
151 D  L  Y  Y  L  M  D  L  S  N  S  M  A  D  D  K  E  K  L  A  S  L  G  V  K  I  A  E  D  M
   AGCACCATCACTAAGAACTTCAAGCTGGGTTTGGTTCCTTTGTGGACAAGGTTGTCATGCCCTACGTCAGTACAGCCCCTAATAAAATT  630
181 S  T  I  T  K  N  F  K  L  G  F  G  S  F  V  D  K  V V M  P  Y  V  S  T  A  P  N  K  I
   AACAGTCCTTGTCCAGGATGTGAGAAGGCTTATGGATTTAGAAACGTTCACCCATTGGACCCAAATGCTACACTGTTCAGGGACAAAGTC  720
211 N  S  P  C  P  G  C  E  K  A  Y  G  F  R  N  V  H  P  L  D  P  N* A  T  L  F  R  D  K  V
   AATGCAGCCAAGGTATCTGGTAACCTTGATGCTCCGGAGGGTGGGTTCGACGCCATCATGCAGGCCATAGCTTGTGAGACAGAGATTGGG  810
241 N  A  A  K  V  S  G  N  L  D  A  P  E  G  G  F  D  A  I  M  Q  A  I  A  C  E  T  E  I  G
   TGGAGGAACCGATCCAGAAGAATGTTGCTGTTCTCCACAGACGCTGGATTTCATTACGCTGGGGACGGAGAACTTGGAGGCATCATTCAA  900
271 W  R  N* R  S  S  R  R  M  L  L  F  S  T  D  A  G  F  H  Y  A  G  D  G  E  L  G  G  I  I  Q
   CCCAATGATGGAAACTGTCATCTTAGTCCTGACGGAATGTACACAGAAAGTTCTAATCAGGACTACCCCTCTATTAGTCAAGTCGCGGTG  990
301 P  N  D  G  N  C  H  L  S  P  D  G  M  Y  T  E  S  S  N  Q  D  Y  P  S  I  S  Q  V  A  V
   AAAGCCAAGGAAAAGAATGTCAACATCATTTTCGCCGTCACCAACGATCAAAAGAACATTTATGATCAGCTCAAGCCAATCATTGCGGGA 1080
331 K  A  K  E  K  N  V  N  I  I  F  A  V  T  N  D  Q  K  N  I  Y  D  Q  L  K  P  I  I  A  G
   TCGGAAACAGGAGTTTTGGCGTCAGACTCACAGAACGTTGTCAAGCTAGTCAGAGACAACTACTTGGCCATCACATCAAAAGTAGAAATG 1170
361 S  E  T  G  V  L  A  S  D  S  Q  N  V  V  K  L  V  R  D  N  Y  L  A  I  T  S  K  V  E  M
   ATTGTTGAAAACTCAGACAATTTGGAGGTGAAATTCAGGACAAAATGTAAAGGAACTGAAGAGAAAGAGACAAACAAGTGTGAGAACTTG 1260
391 I  V  E  N  S  D  N  L  E  V  K  F  R  T  K  C  K  G  T  E  E  K  E  T  N  K  C  E  N  L
   GCCATTGGAGGATCTGTGGATTTCAGTGTGACAGTGGAAGTGAAGAGCTGCCCCCCCAAAGGTGAAGAGGAGAGGACCCTCAGGATCAAA 1350
421 A  I  G  G  S  V  D  F  S  V  T  V  E  V  K  S  C  P  P  K  G  E  E  E  R  T  L  R  I  K
   CCAGTCGGACTGTATGATGATTTGACTGTCAAACTGAAGCTCATGTGTCAGTGTGACTGCGAGTCCCCAAAGCAAATGGAAGACAACAAG 1440
451 P  V  G  L  Y  D  D  L  T  V  K  L  K  L  M  C  Q  C  D  C  E  S  P  K  Q  M  E  D  N  K
   AACCACGAGAAATGTAATGGAAACGGGACGTACGTGTGTGGAATGTGCGTGTGTAACGAGCCGTACTTTGGAGACTATTGTGACTGTGAC 1530
481 N  H  E  K  C  N  G  N* G  T  Y  V  C  G  M  C  V  C  N  E  P  Y  F  G  D  Y  C  D  C  D
   AAGGGCACCGGGACCATCGCTGACAAGGAGTCGGAGTGTATCCAGGACAAGAACACGACCATCATCTGTAACGGCCGGGGAGAATGTAAC 1620
511 K  G  T  G  T  I  A  D  K  E  S  E  C  I  Q  D  K  N* T  T  I  I  C  N  G  R  G  E  C  N
   TGCGGAACGTGCACGTGTCGGGAGAGACAGAAGGGCACCAACCACTTCTACACGGGCAGATACTGCGAGTGTGACGATTACAGCTGTCCC 1710
541 C  G  T  C  T  C  R  E  R  Q  K  G  T  N  H  F  Y  T  G  R  Y  C  E  C  D  D  Y  S  C  P
   TACTACGCTGGGCTGATCTGTGGAGGTCTGGGTCGCGGACAGTGTGACTGTGGAAACTGTAAGTGTAACGCCGGTTTCAATGGCACGAAC 1800
571 Y  Y  A  G  L  I  C  G  G  L  G  R  G  Q  C  D  C  G  N  C  K  C  N  A  G  F  N* G  T  N
   TGCGGATGTAACACCGACAACTCTACCTGTATGTACAATGGATTGCTGTGTAATGATAAAGGAACTTGTGAGTGTGGCAAGTGTACCTGT 1890
601 C  G  C  N  T  D  N* S  T  C  M  Y  N  G  L  L  C  N  D  K  G  T  C  E  C  G  K  C  T  C
   ACTGATCCTAAGTACTTTGGACCCCAGTGTCAGGAATGTGATAACTGTGGCCAGGAGCAATGTCGTACCCACCAGGACTGTGCGCTGTGT 1980
631 T  D  P  K  Y  F  G  P  Q  C  Q  E  C  D  N  C  G  Q  E  Q  C  R  T  H  Q  D  C  A  L  C
   AACAGAACCAATGCCGGGGTACTGACCAAGGAACAGTGTGAAAAAGAGTGCTCCCATACCACTGCCGTCGACAAAATCAGAAATGGCATC 2070
661 N* R  T  N  A  G  V  L  T  K  E  Q  C  E  K  E  C  S  H  T  T  A  V  D  K  I  R  N  G  I
   ACTAATTGCGAGTACGTAGACCAGAACGGCTGCTTTATTTACTTTACCTATTTCTATGACGATGATGGCACACTGAGGGTAGAAGTCCAA 2160
691 T  N  C  E  Y  V  D  Q  N  G  C  F  I  Y  F  T  Y  F  Y  D  D  D  G  T  L  R  V  E  V  Q
   AAAGAGCCAGAGTGTCCCCCCGAGGTCAACGTCCTTGCCATAGTCCTGGGGGTGATAGCGGGCATCGTGTTCTTTGGGATCATCCTCCTC 2250
721 K  E  P  E  C  P  P  E  V  N  V  L  A  I  V  L  G  V  I  A  G  I  V  F  F  G  I  I  L  L
   CTGATCTGGAAACTATTCACCACCATTAGTGATAAGAGAGAGCTGGCCAGGTTCGAAAAGGAGGCCATGAACGCCCGATGGGATACGGGA 2340
751 L  I  W  K  L  F  T  T  I  S  D  K  R  E  L  A  R  F  E  K  E  A  M  N  A  R  W  D  T  G
   GAAAATCCTATCTACAAGCAGGCTACATCCACCTTTGTCAACCCCACCTACAGGCAGTGAgaaccctcttttacagcagaggggggaaat 2430
781 E  N  P  I  Y  K  Q  A  T  S  T  F  V  N  P  T  Y  R  Q  stop
   caagagcccagaacagccatggagattataacatgcagctaggcaggaaaaaaaaaaaaaaaaa                          2496
```

Fig. 2. cDNA sequence and deduced amino acid translation of β_{CGH} (A) and schematic diagram of translated β_{CGH} showing conserved domains and motifs by in silico analysis (B). A: The open reading frame (ORF) is in uppercase letters and the 3′ and 5′ untranslated nucleotides are in lowercase. Nucleotides are numbered on the right from the 5′ end (non-bold text) and amino acid residues on the left (bold text) from the initial ATG-encoded methionine. Amino acid residues are marked by characters in bold. The putative signal peptide is underlined with a solid line; the putative ligand-binding domain with a dashed line; and the putative transmembrane domain with a double line. Eight putative N-glycosylation sites are indicated with asterisks. B: β_{CGH} comprises signal sequence, extracellular, transmembrane, and cytoplasmic domains in its structure. The extracellular domain contains a ligand-binding domain (LBD) including a metal ion-dependent adhesion site (MIDAS), eight N-glycosylation sites, a tyrosine kinase phosphorylation site, two cysteine-rich repeat signatures, two epidermal growth factor (EGF)-like domain signature 1, and two EGF-like domain signature 2. The cytoplasmic domain contains a putatively conserved membrane proximal region motif, two protein kinase C (PKC) phosphorylation sites, and two NPXY motifs. Numbers are the positions of amino acid residues in A.

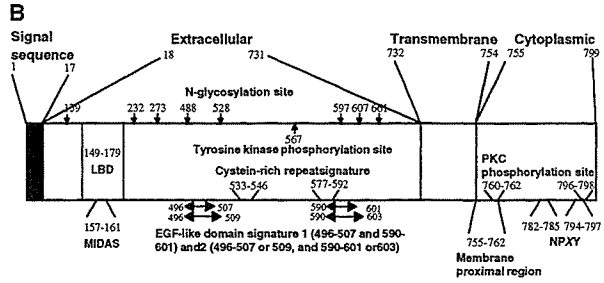

Fig. 2 (*continued*)

[34], was presumed to be positioned from the 755th to 762nd amino acid residues (LFTTISDK).

In our preliminary experiments, the full-length ORF was amplified by RT-PCR and the recombinant β_{CGH} was shown to be expressed in vitro in the amplified product; confirming that the putative ORF sequence assembled from the subcloned fragments was correct and able to be translated. As a result, 115.4-kDa of

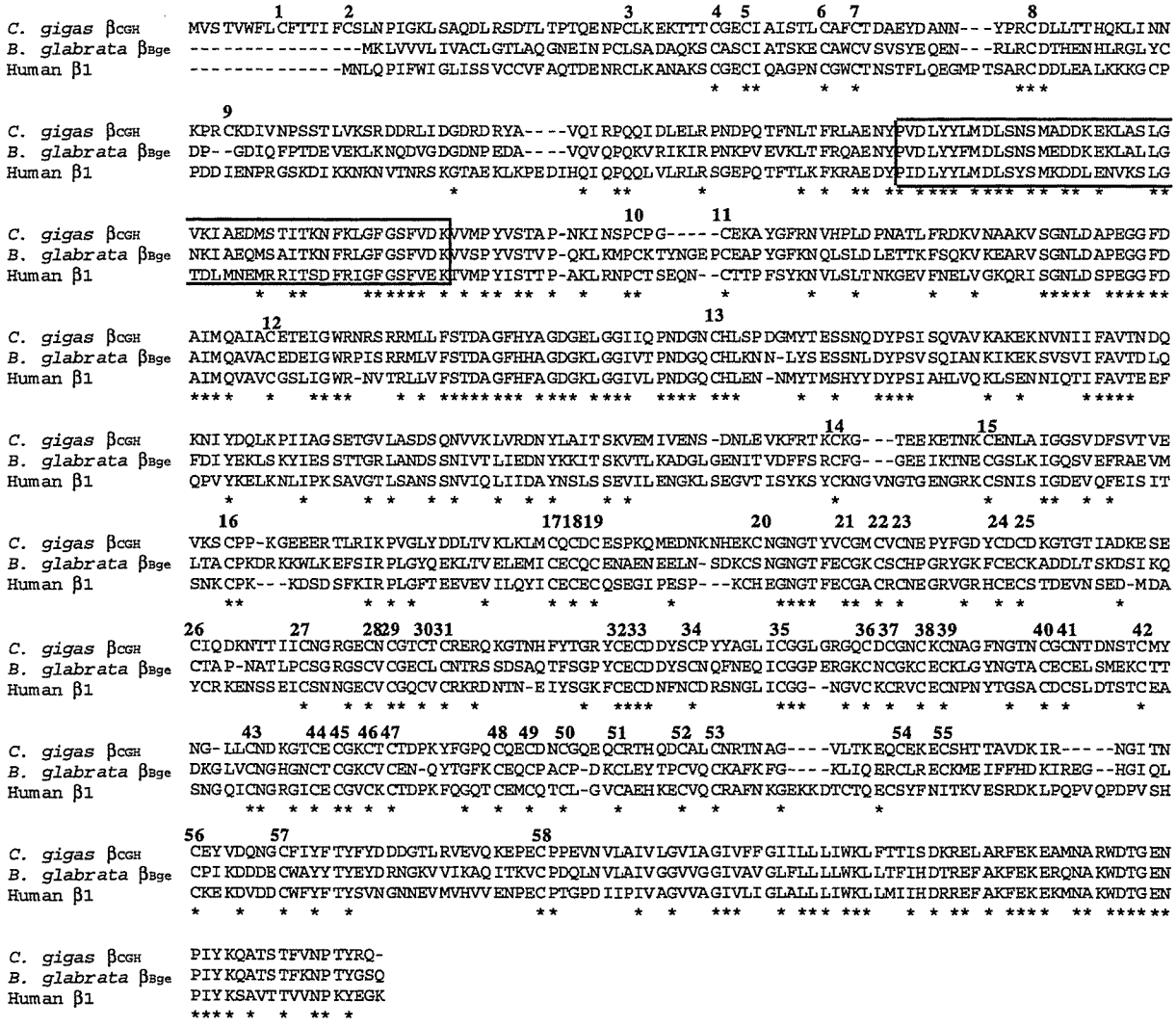

Fig. 3. Multiple alignments of the amino acid sequences of β integrin ORFs. β_{CGH} is aligned with *B. glabrata* β_{Bge} (AF060203) and human β_1 (X07979). Dashes represent gaps. The putative ligand-binding domain is boxed. Numbers above sequences indicate the 58 cysteine residues. Asterisks indicate similar amino acid residues among the three sequences.

glutathione-*S*-transferase (GST)-tagged fusion protein was detected by Western blotting using anti-GST antibody (data not shown).

3.2. Similarity to other β integrins

Comparison with information in the BLAST database revealed a significant similarity to other β integrins. β_{CGH} was compared for similarity with human β_{1-8} and 20 other known invertebrate β integrins. The highest similarity (47%) was with the β_{Bge} integrin of *Biomphalaria glabrata*, a gastropod molluscan species. In addition, human β_1 showed the closest similarity (41%) in human β_{1-8}. When the amino acid sequence of β_{CGH} was aligned with those of β_{Bge} and human β_1 using ClustalW [35], the putative LBD, transmembrane domain and cytoplasmic domain of β_{CGH} were well conserved (Fig. 3).

3.3. Northern blot analysis

Expression of mRNA encoding β_{CGH} was also confirmed by Northern blot analysis using fragment 3, which is highly conserved throughout other β integrins; though the probe detected only approximately 6 kb of mRNA encoding β_{CGH} (Fig. 4). In addition, expression of mRNA encoding GAPDH as a positive control was detected at approximately 1.1 kb (Fig. 4).

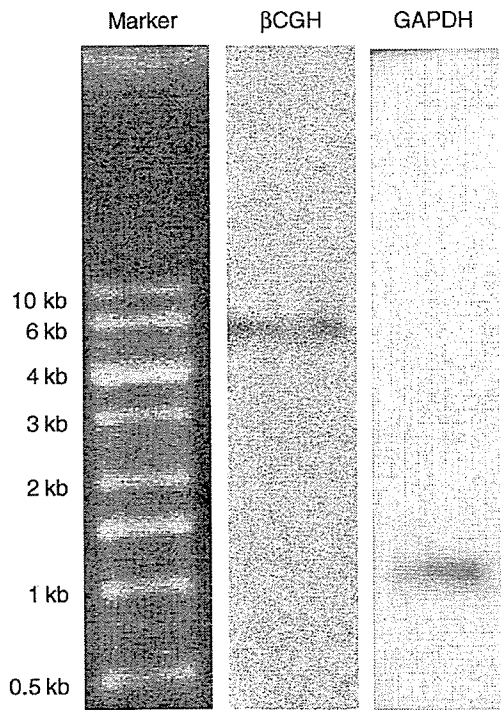

Fig. 4. Northern blot analysis of expressed β_{CGH} and GAPDH mRNAs. A single band is detected at approximately 6 and 1.2 kb at β_{CGH} and GAPDH lanes, respectively. Markers were separated from the sample lane after electrophoresis and visualized by staining with ethidium bromide.

3.4. Quantification of β_{CGH} mRNA expression in C. gigas hemocyte subpopulations

Sorted granulocyte, hyalinocyte and agranulocyte fractions were used to investigate the expression levels of β_{CGH} mRNA. Expression levels of β_{CGH} mRNA in each hemocyte subpopulation were normalized by expression of GAPDH mRNA. Quantitative real-time RT-PCR analysis demonstrated that the expression level of β_{CGH} mRNA in the hyalinocyte fraction was significantly higher than that in the granulocyte and agranulocyte fractions (3.8- and 11.0-fold, respectively; Fig. 5). In addition, the level within the granulocyte fraction was 2.9-fold higher than that in the agranulocyte fraction, although the difference was not significant.

3.5. Morphological characterization of C. gigas hemocyte subpopulations

Using sorted hemocyte subpopulations, we could distinguish each hemocyte subpopulation by May-Grünwald and Giemsa staining as follows: (1) granulocytes: these cells had eosinophilic cytoplasm and contained many basophilic granules throughout their cytoplasm (Fig. 6B); (2) hyalinocytes: the cytoplasm of these cells were stained light pink, and

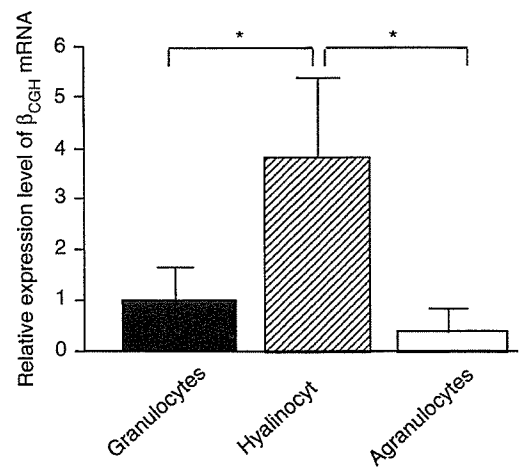

Fig. 5. Relative quantitative expression of β_{CGH} mRNA in granulocyte, hyalinocyte, and agranulocyte fractions according to real-time RT-PCR. For quantitative comparisons, the value within the granulocyte fraction was defined as 1. The relative values represent the mean+SD ($n=3$). Significant differences ($^*p<0.05$) were determined by Tukey's multiple comparison test.

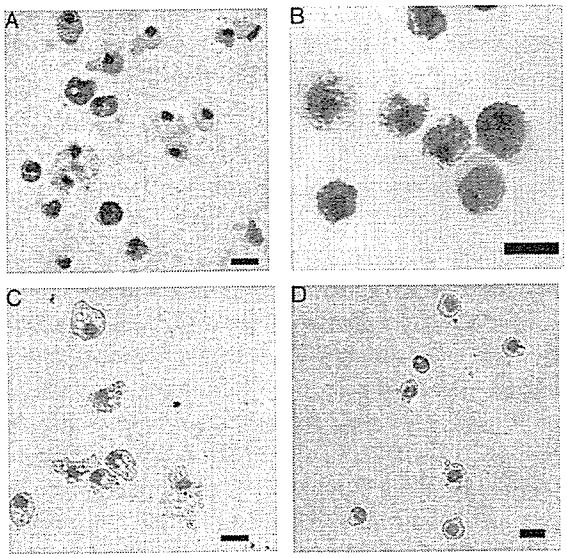

Fig. 6. Micrographs of cytospun specimens stained with May-Grünwald and Giemsa. Hemocyte subpopulations from *C. gigas* were prepared by a cell-sorter. A: Intact hemocytes contained in hemolymph. B–D: Sorted granulocytes, hyalinocytes, and agranulocytes. Scale bars are 10 μm.

no granules and many small vacuoles were present into the cytoplasm (Fig. 6C); (3) agranulocytes: these cells were smaller than the other two types of hemocyte subpopulations, and their cytoplasm were stained basophilic and a low ratio to nucleus (Fig. 6D).

3.6. Immuno-reactivities of anti-integrin antibodies against C. gigas hemocytes

Because of the high conserved sequences of β_{CGH}, it was expected that polyclonal antibodies for human β_1-associated integrins would be useful for the detection and functional analyses of *C. gigas* integrins on hemocyte surfaces. Therefore, immuno-reactivities were tested by immunocytochemistry and Western blotting using anti-integrin $\alpha_5\beta_1$ and/or anti-integrin β_1 antibodies.

When immunocytochemistry was first performed using anti-integrin $\alpha_5\beta_1$ antibody, specific immunoreaction was detected in all subpopulations of *C. gigas* hemocytes (Fig. 7A). In the control cases treated with normal goat IgG or without primary antibody, most hemocytes were negative as shown in Fig. 7B.

Subsequently, Western blot analyses were performed using both anti-integrin $\alpha_5\beta_1$ and anti-integrin β_1 antibodies (Fig. 7C and D). Two specific bands (approximately 100 kDa and over 200 kDa) were detected by anti-integrin $\alpha_5\beta_1$ antibody (Fig. 7C). When using anti-integrin β_1 antibody, only an approximately

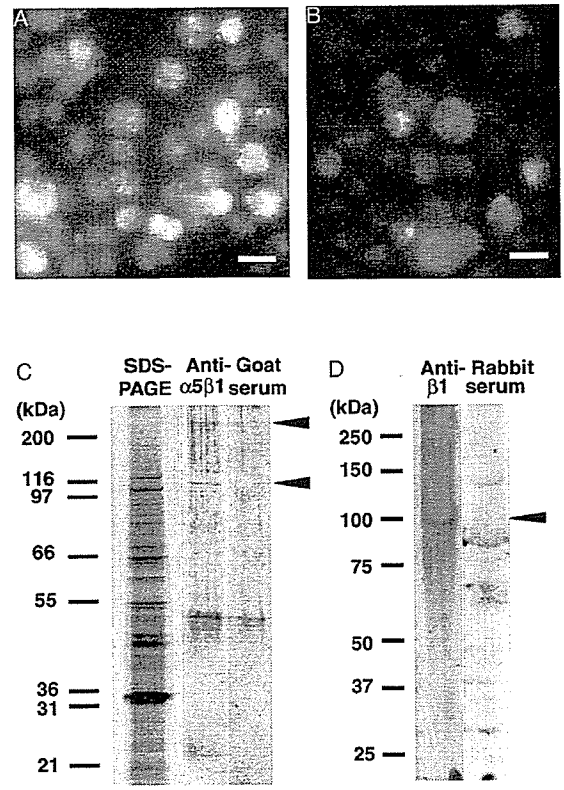

Fig. 7. Immuno-reactivities of *C. gigas* hemocytes with anti-integrin antibodies. Anti-integrin $\alpha_5\beta_1$ polyclonal antibody recognizes the extracellular domain of human $\alpha_5\beta_1$ integrin, and anti-integrin β_1 polyclonal antibody recognizes the cytoplasmic domain of human β_1 integrin. A and B: Immunocytochemistry of *C. gigas* hemocytes with goat anti-integrin $\alpha_5\beta_1$ polyclonal antibody (A) and normal goat IgG (B). Immunoreactions of anti-integrin $\alpha_5\beta_1$ antibody were detected in all subtypes of *C. gigas* hemocytes (A), while normal goat IgG showed almost negative immunoreactions (B). Similarly, a secondary antibody alone also showed negative immunoreactions like those shown in B. Scale bars are 10 μm. C and D: Western blotting with goat anti-integrin $\alpha_5\beta_1$ (C) and rabbit anti-integrin β_1 (D) polyclonal antibodies. Goat anti-integrin $\alpha_5\beta_1$ polyclonal antibody specifically detected over 200 kDa and approximately 100 kDa bands (closed triangles) while normal goat serum did not react with these bands (C). Rabbit anti-integrin β_1 polyclonal antibody specifically detected an approximately 100 kDa band (closed triangle), while normal rabbit serum did not react with the band (D).

100 kDa protein was specifically detected (Fig. 7D). These detected proteins were not detected by normal goat and rabbit sera as negative controls.

3.7. Involvement of integrins in phagocytosis of C. gigas hemocytes against zymosan particles

Zymosan particles are well phagocytosed by circulating hemocytes of oyster species [36]. Therefore, we initially used zymosan particles as model particles for this phagocytosis assay to characterize the phagocytic ability of each hemocyte subpopulation,

and investigated the involvement of integrins in the phagocytosis. Based on the morphological characteristics with the sorted hemocyte specimens, we distinguished each hemocyte subpopulation from the intact hemocytes containing all subpopulations in the phagocytosis assay. Granulocytes and especially hyalinocytes spread with well-developed pseudopodia and contained many zymosan particles in their cytoplasm (Fig. 8A and B), while agranulocytes were smaller expanding cells, round in shape (Fig. 8C). The granulocytes and hyalinocytes potentially possessed high phagocytic abilities, e.g. PRs and PIs of oyster BSS-pre-treated granulocytes and hyalinocytes against zymosan particles were 92.0% and 4.3 (oyster BSS-pre-treated granulocytes), and 75.7% and 7.5 (oyster BSS-pre-treated hyalinocytes), respectively (Fig. 8D and E).

To assess the contribution of integrins expressed on the surface membranes of granulocytes and hyalinocytes to phagocytosis against zymosan particles, we examined the phagocytic abilities of hemocytes that were pre-treated with the anti-integrin $\alpha_5\beta_1$ antibody on their surface membrane to block integrin-zymosan interactions. Interestingly, the phagocytic ability of hyalinocytes against zymosan particles was markedly inhibited by blocking with an anti-integrin $\alpha_5\beta_1$ antibody, whereas granulocytes retained their high phagocytic ability. PR of hyalinocytes pre-incubated with anti-integrin $\alpha_5\beta_1$ antibody was reduced to 40.9% and was significantly lower than that of normal goat IgG-treated (68.6%) and oyster BSS-treated hyalinocytes (75.7%) (Fig. 8D, hyalinocytes). PI of the hyalinocytes also significantly decreased to 4.8 compared to that of normal goat IgG- or oyster BSS-treated hyalinocytes (7.1 and 7.5, respectively) (Fig. 8E, hyalinocytes). Although the anti-integrin $\alpha_5\beta_1$ antibody significantly reduced PR of granulocytes against zymosan particles (82.5%) compared to that of oyster BSS-treated granulocytes (92.0%), no significant difference was detected for the normal IgG-treated granulocytes (88.3%), and the inhibitory effects were less marked (Fig. 8D, granulocytes). Furthermore, no decrease of PI was measured with pre-incubation of anti-integrin $\alpha_5\beta_1$ antibody in the granulocytes (Fig. 8E, granulocytes). In agranulocytes, no or little phagocytosis was found under any of the treatments (Fig. 8D and E, agranulocytes).

3.8. Effect of integrin-dependent binding on phagocytic ability of C. gigas hemocytes

We assessed quantitative integrin-dependent phagocytic ability among *C. gigas* hemocyte subpopulations using anti-integrin $\alpha_5\beta_1$ antibody-conjugated microspheres (integrin-microspheres). A light micrograph of *C. gigas* hemocytes fixed after 30 min incubation with integrin-microspheres showed that numerous microspheres were contained within hemocyte vesicles of the hemocytes and/or attached onto the plasma membrane of hemocytes (Fig. 9A).

When a panel of microspheres was provided to the hemocyte layer, hyalinocytes significantly phagocytosed the integrin-microspheres (PR 38.4%) rather than the normal goat IgG-conjugated microspheres (IgG-microspheres, PR 20.3%) or oyster BSS-treated microspheres (PR 20.0%). PI of hyalinocytes against integrin-microspheres also increased to 4.3 compared to the IgG-microspheres (1.8) and oyster BSS-treated microspheres (2.3) (Fig. 9C). In contrast, PR and PI of granulocytes showed high values against IgG-microspheres (PR 77.0% and PI 6.4), and oyster BSS-treated microspheres (PR 78.5% and PI 6.9). However, no significant enhancement of phagocytic ability was observed by the integrin-microspheres (PR 83.6% and PI 8.8). Integrin-microspheres had no effect on the enhancement of the phagocytic ability in agranulocytes as shown by the low PR (0.3%) and a small PI (1.7).

4. Discussion

In this study, we presented the first cloning of the integrin β subunit gene from *C. gigas* hemocytes. The revealed sequence was deemed an authentic member of the integrin family, because the molecular weight, structural features and similarities to other β integrins were well conserved; thus, we designated this molecule as β_{CGH}. This is the first study to report cloning of β integrin-encoding cDNA in bivalve cells. In addition to RT-PCR during the cloning process, the expression of β_{CGH} mRNA was also detected by the Northern blot analysis, although there seems to be a discrepancy in the size between ORF (2.4 kb) and mRNA (approximately 6 kb) of β_{CGH}. However, in the case of snail β integrin (β_{Bge}), its encoding ORF and mRNA had been shown to have respective sizes of 1971 bases and approximately 8 kb [6]. Therefore, in molluscs, mRNA encoding a β integrin is assumed to contain large 5′ and/or 3′ untranslated regions.

Phylogenetic analysis, including β_{CGH}, had already been reported by Miyazawa and Nonaka [19]. They found that β_{CGH} belongs to one of the clusters consisting of invertebrate β integrins such as *B. glabrata* β_{Bge} (AF060203), *Pseudoplusia includens* β_{Pi1} (AY237588), *Drosophila melanogaster* β_{PS} (J03251), *Anopheles gambiae* β_{PS} (AJ292755),

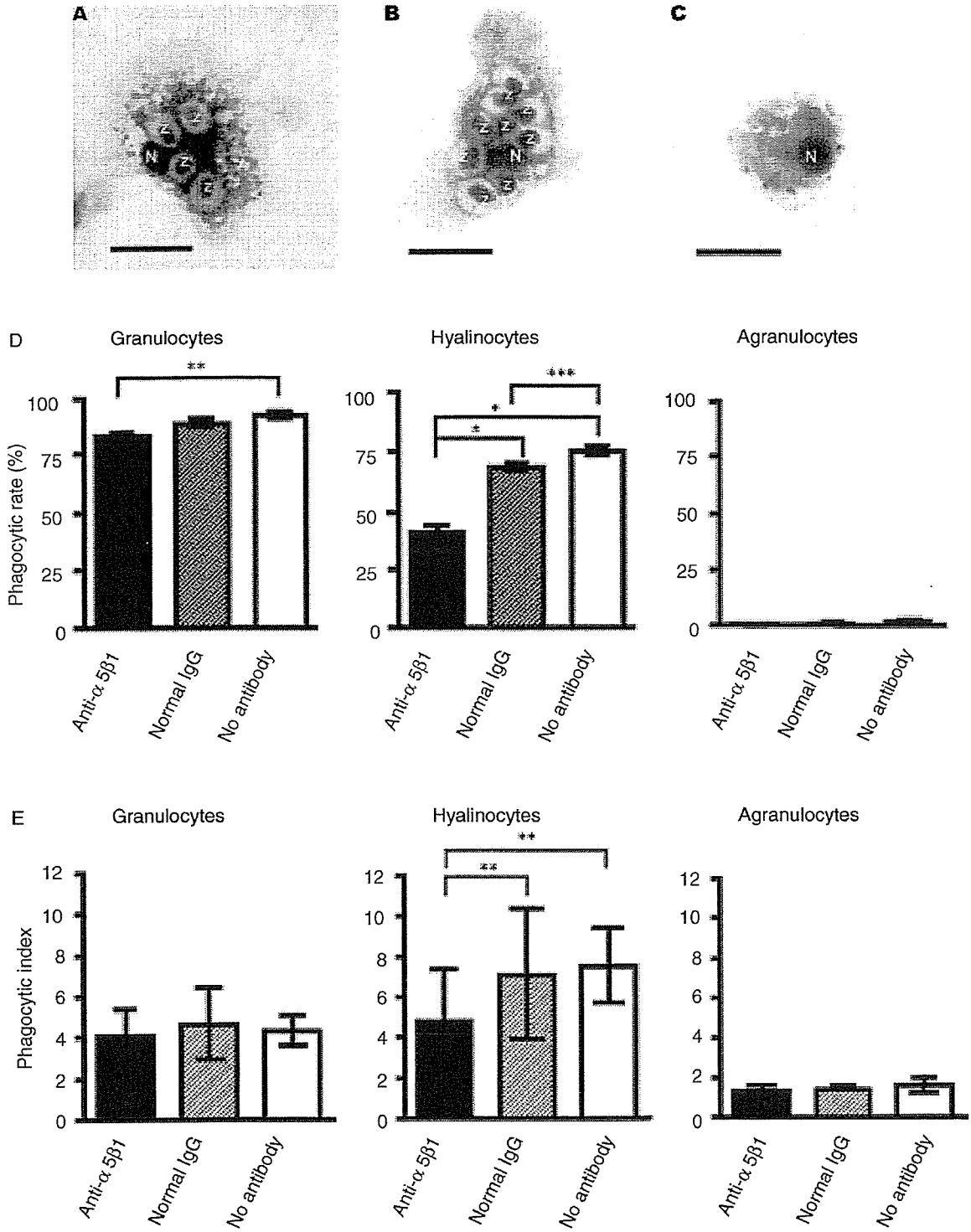

Fig. 8. Inhibitory effects on the phagocytic ability against zymosan particles by blocking with anti-integrin $\alpha_5\beta_1$ antibody to the surface membranes of *C. gigas* hemocytes. A–C: Photomicrographs of spreading and/or phagocytosing hemocytes (×1000). A: Granulocyte ingesting zymosan particles (z). B: Hyalinocyte ingesting zymosan particles (z). C: Agranulocyte. N: Nucleus of each hemocyte. Scale bars are 10 μm. D: Phagocytic rate (mean+SE, $n=5$) of granulocytes, hyalinocytes, and agranulocytes, which were pre-treated with anti-integrin $\alpha_5\beta_1$ antibody, normal IgG, and oyster BSS alone. E: Phagocytic index (mean+SE, $n=5$) of each hemocyte subpopulation described above. Significant differences ($^*p<0.001$, $^{**}p<0.01$, $^{***}p<0.05$) were determined by Tukey's (D) or Newman–Keuls (E) multiple comparison tests.

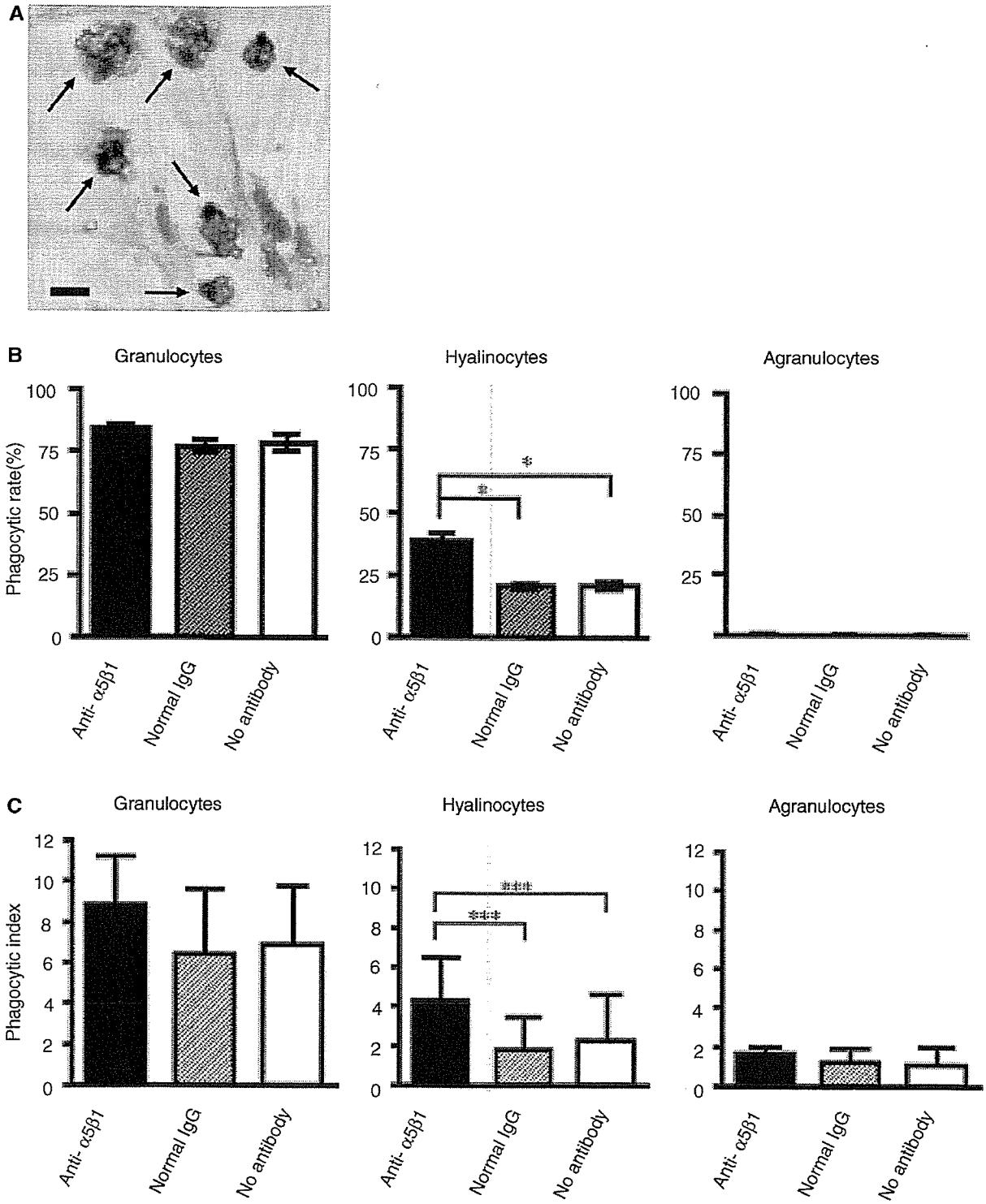

Fig. 9. Effects on phagocytic ability of *C. gigas* hemocytes by particle-binding via integrins. A: Photomicrograph of whole hemocytes phagocytosing anti-integrin $\alpha_5\beta_1$ antibody-conjugated microspheres. Arrows are hemocytes that ingested microspheres. Scale bar is 10 μm. B: Phagocytic rate (mean ± SE, $n=5$) of granulocytes, hyalinocytes, and agranulocytes against anti-integrin $\alpha_5\beta_1$ antibody- and normal IgG-conjugated microspheres and oyster BSS-treated microspheres. C: Phagocytic index (mean + SE, $n=5$) of each hemocyte subpopulation against three kinds of microspheres described above. Significant differences ($^*p<0.001$, $^{***}p<0.005$) were determined by Tukey's (B) or Newman–Keuls (C) multiple comparison tests.